

Beyond Diagonal Intelligent Reflecting Surface Aided Integrated Sensing and Communication

Shuo Zheng, *Graduate Student Member, IEEE*, and Shuowen Zhang, *Senior Member, IEEE*

Abstract—Beyond diagonal intelligent reflecting surface (BD-IRS) is a new promising IRS architecture for which the reflection matrix is not limited to the diagonal structure as for conventional IRS. In this paper, we study a BD-IRS aided uplink integrated sensing and communication (ISAC) system where sensing is performed in a device-based manner. Specifically, we aim to estimate the *unknown* and *random* location of an active target based on its uplink probing signals sent to a multi-antenna base station (BS) as well as the known prior distribution information of the target's location. Multiple communication users also simultaneously send uplink signals, resulting in a challenging mutual interference issue between sensing and communication. We first characterize the sensing performance metric by deriving the *posterior Cramér-Rao bound (PCRB)* of the mean-squared error (MSE) when prior information is available. Then, we formulate a BD-IRS reflection matrix optimization problem to maximize the minimum expected achievable rate among the multiple users subject to a constraint on the PCRB as well as the lossless and reciprocal constraints on the BD-IRS reflection matrix. The formulated problem is non-convex and challenging to solve. To tackle this problem, we propose a penalty dual decomposition (PDD) based algorithm which can find a high-quality suboptimal solution with polynomial-time complexity. In addition, we propose and optimize a time-division multiple access (TDMA) based scheme which removes the sensing-communication mutual interference. Numerical results verify the effectiveness of the proposed designs and provide useful design insights such as the optimal choice of multiple access scheme.

Index Terms—Beyond diagonal intelligent reflecting surface (BD-IRS), beyond diagonal reconfigurable intelligent surface (BD-RIS), integrated sensing and communication (ISAC), posterior Cramér-Rao bound (PCRB).

I. INTRODUCTION

The sixth-generation (6G) wireless networks are expected to support a wide range of advanced applications, including autonomous driving, smart cities, and real-time monitoring. These applications often require both high-accuracy sensing and reliable communication. In this context, integrated sensing and communication (ISAC) has emerged as a promising technology, which goes beyond traditional communication and enables real-time collection, analysis, and processing of data from a variety of sensing anchors [2]. By integrating these functions, ISAC offers significant advantages in terms of spectrum and energy efficiency, as well as cost reduction. This approach not only improves sensing accuracy through the ubiquitous communication networks but also enhances

network performance by utilizing the environmental information gathered from sensing, such as the locations of objects or obstacles. As a result, ISAC plays a crucial role in the evolution of 6G, and is considered as a key enabler of more intelligent and resource-efficient wireless networks [3], [4].

In recent years, intelligent reflecting surfaces (IRSs), also known as reconfigurable intelligent surfaces (RISs), and their diverse variants have gained increasing attention [5]–[8]. An IRS is a reconfigurable metasurface composed of numerous reflecting elements capable of controlling signal propagation. By leveraging this capability, IRS can enhance communication reliability, reduce interference, and extend communication coverage, even in challenging environments. This technology opens the door to dynamic and controllable wireless propagation environments, leading to fully reconfigurable networks. By dynamically manipulating the wireless environment, IRS improves both communication and sensing capabilities [2], [9]–[11], thereby augmenting ISAC systems [12], [13]. Numerous research efforts have focused on IRS-aided ISAC systems [14]–[18]. For instance, [14] investigated the joint waveform and discrete IRS phase shift design in ISAC systems. In [15], a heterogeneous 6G sensing system was proposed, which integrates active and passive anchors, with IRSs serving as cost-effective passive anchors that facilitate joint sensing with base stations (BSs) being the active anchors. In [16], physical-layer security in IRS-aided ISAC systems was studied, where active and passive beamforming were jointly designed to enhance ISAC performance while suppressing information leakage. [17] considered a device-based sensing scenario where an active target sends uplink signals to the BS with the help of an IRS. Furthermore, [18] introduced a simultaneously transmitting and reflecting surface (STARS) enabled ISAC framework, where STARS divides space into distinct sensing and communication areas.

However, the diagonal structure of the reflection matrix of conventional IRS limits its potential performance gains. Recently, a novel IRS architecture, termed *beyond diagonal IRS (BD-IRS)* [19], [20], also known as non-local IRS [21], [22] or beyond diagonal RIS (BD-RIS), has been proposed. Unlike diagonal IRS, BD-IRS allows inter-connections among its elements, thereby resulting in a beyond diagonal reflection matrix and offering greater design flexibility. By exploiting this property, BD-IRS can manipulate both the amplitude and phase of incident signals, which unlocks new opportunities for enhancing system performance. Thanks to the beyond diagonal structure of reflection matrix, BD-IRS is expected to outperform conventional IRS in many aspects. To date, several studies have explored the design and optimization of

This paper will be presented in part at the IEEE Workshop on Signal Processing and Artificial Intelligence for Wireless Communications (SPAWC), Surrey, United Kingdom, July 2025 [1].

The authors are with the Department of Electrical and Electronic Engineering, The Hong Kong Polytechnic University, Hong Kong SAR, China (e-mail: shuo.zheng@connect.polyu.hk; shuowen.zhang@polyu.edu.hk).

BD-IRS in various scenarios [20], [23]–[27]. The concept and modeling of BD-IRS architecture were first introduced in [20] and then further studied in [23]. [24] investigated the joint design of transmit precoders and BD-IRS reflection matrix to maximize the sum-rate in multi-user multiple-input-single-output (MISO) systems and showed BD-IRS’s advantages over various architectures or operating modes. Despite its performance benefits, BD-IRS introduces additional circuit design complexity. To balance circuit complexity with performance, novel modeling approach, architecture design, and optimization framework for BD-IRS were proposed in [23] based on graph theory. Furthermore, the multi-sector BD-IRS concept was introduced in [25], while [26] studied the modeling and optimization of BD-IRS with the existence of mutual coupling. In [27], the BD-IRS reflection matrix was designed to minimize transmit power and maximize energy efficiency, subject to individual signal-to-interference-plus-noise ratio (SINR) constraints in a downlink multi-user MISO system. In [28], multiple BD-IRSs were exploited to assist the multiple access system in a cooperative way. A distributed beamforming design with low information exchange overhead was proposed to improve the sum-rate. BD-IRS has also been explored for a wide range of applications, including rate splitting multiple access [29], [30], unmanned aerial vehicles [31], mobile edge computing [32], simultaneous wireless information and power transfer [33], physical-layer security [34], and non-orthogonal multiple access [35].

In the context of ISAC, several studies have explored BD-IRS aided ISAC systems [36]–[41]. In [36], the joint beamforming design in a downlink ISAC system was investigated to maximize throughput while satisfying a sensing signal-to-noise ratio (SNR) constraint. [37] focused on the transmit power minimization problem under similar settings. In [38], a discrete phase setting was considered, and the maximization problem of the weighted sum of communication and sensing SNRs was studied. Additionally, [39] leveraged BD-IRS operating in hybrid modes to enable full-space coverage. For multi-target scenarios, [39] investigated a max-min signal-to-clutter-plus-noise ratio (SCNR) problem subject to communication rate constraints. [36]–[39] utilized SNR or SCNR of the echo signal as the sensing performance metric, which, however, cannot reflect the error performance explicitly. Another widely recognized metric for sensing performance is the Cramér-Rao bound (CRB), which provides an analytical lower bound for the mean-squared error (MSE). In [40], CRB was adopted to characterize the sensing performance of a multi-sector BD-IRS aided sensing system. Moreover, [41] proposed a novel transmitter architecture for a BD-IRS aided millimeter wave ISAC system and designed the joint beamforming to simultaneously maximize the sum-rate and minimize the largest eigenvalue of the CRB matrix.

However, CRB is only applicable to *deterministic* parameters and is determined by their true values. In practice, the parameters to be estimated are often *unknown* and *random*, whose distributions can be known via statistical information [42]–[50]. A new performance metric termed as *posterior Cramér-Rao bound (PCRB)* [42]–[50] or Bayesian Cramér-Rao bound (BCRB) [17], [51] serves as a lower bound on

the MSE for sensing exploiting prior distribution information. Unlike CRB, PCRB is only a function of the prior distributions and does not depend on the true parameter values. Several prior studies have investigated PCRB minimization in ISAC systems [17], [42]–[52]. Nevertheless, how to optimize the performance of the BD-IRS aided ISAC or sensing systems with available prior distribution information of parameters still remains open for investigation, which motivates our study.

In this paper, we investigate the BD-IRS reflection optimization in a BD-IRS aided multi-user uplink ISAC system, where a multiple-antenna BS simultaneously serves multiple single-antenna communication users in the uplink and senses the *unknown* and *random* location information of a target. The target is active and transmits probing signals to the BS for device-based sensing. The BS senses the target’s location based on the received signals and the known probability density function (PDF) of the target’s location. There are three main challenges in this scenario. *Firstly*, in downlink monostatic device-free sensing where the BS performs downlink communication and sensing based on the target-reflected echo signals, communication signals will not cause interference to sensing as they are known at the BS. However, in the studied uplink case, there exists *mutual interference* between sensing and communication, as both the communication signals and target’s location are *unknown* at the BS. This thus calls for more powerful interference management via reflection optimization to strike an optimal balance between sensing and communication. *Secondly*, the new general BD-IRS reflection matrix structure calls for new characterizations of the sensing performance and new optimization techniques as the results for conventional diagonal reflection matrices are not directly applicable. *Thirdly*, how to judiciously design the BD-IRS reflection matrix to prioritize a range of possible locations with high probabilities under its structural constraints is a new challenging task.

Motivated by the above challenges, we make the following contributions in this paper:

- Firstly, we characterize the PCRB for BD-IRS aided uplink ISAC as an explicit and tractable function of the BD-IRS reflection matrix, where the interference caused by communication is taken into account. We also derive a tractable lower bound of the expected achievable rate for each user averaged over the random interference caused by random target locations.
- Next, we formulate an optimization problem for the BD-IRS reflection matrix to maximize the minimum (approximate) expected communication rate among all users, while ensuring the sensing PCRB is below a threshold. This problem is highly non-convex and challenging due to the fractional expressions of communication rates and PCRB with mutual interference, as well as the structural constraints on the BD-IRS reflection matrix. To tackle this problem, we propose a penalty dual decomposition (PDD) [53] based algorithm to obtain a high-quality suboptimal solution with polynomial-time complexity. The proposed algorithm is also extended to the sensing-only case for PCRB minimization.
- Then, motivated by the potential limitation of the studied

space-division multiple access (SDMA) scheme in mitigating severe interference, we propose a time-division multiple access (TDMA) scheme, where the optimal time allocation is derived in closed form.

- Finally, we provide extensive numerical results to validate the performance of the proposed scheme. The proposed algorithm is observed to converge fastly, and achieve superior performance compared with its conventional diagonal IRS counterparts and various benchmark schemes. Moreover, it is observed that TDMA may outperform SDMA in scenarios with heavy mutual interference between sensing and communication, e.g., when the user is located near the highly-probable locations of the target.

The remainder of this paper is organized as follows. Section II presents the BD-IRS aided uplink ISAC system model. Section III derives the PCRB to characterize the sensing performance. Section IV formulates the problem. Section V proposes a suboptimal solution via a PDD-based algorithm. Section VI further proposes and optimizes a TDMA-based scheme. Numerical results are provided in Section VII. Finally, Section VIII concludes this paper.

Notations: Vectors and matrices are denoted by boldface lower-case letters and boldface upper-case letters, respectively. $\mathbb{R}^{N \times M}$ and $\mathbb{C}^{N \times M}$ represent the space of $N \times M$ real matrices and $N \times M$ complex matrices, respectively. For a complex scalar x , $|x|$ and $\Re\{x\}$ denote the absolute value and the real part, respectively. For a vector \mathbf{x} , $\|\mathbf{x}\|$ and x_i denote the l_2 norm and the i -th entry, respectively. For a matrix \mathbf{X} , \mathbf{X}^T , \mathbf{X}^* , \mathbf{X}^H , $\|\mathbf{X}\|_F$, $\|\mathbf{X}\|_\infty$, $X_{i,j}$, $\text{rank}(\mathbf{X})$, $\text{vec}(\mathbf{X})$, and $\text{vech}(\mathbf{X})$ denote the transpose, conjugate, conjugate transpose, Frobenius norm, infinity norm, (i, j) -th entry, rank, vectorization, and half-vectorization, respectively. $\text{vec}^{-1}(\mathbf{X})$ represents inverse operation of vectorization such that $\text{vec}^{-1}(\text{vec}(\mathbf{X})) = \mathbf{X}$. $\text{tr}(\mathbf{S})$, $\det(\mathbf{S})$, and \mathbf{S}^{-1} represent the trace, determinant, and inverse of a non-singular matrix \mathbf{S} , respectively. The $M \times M$ identity matrix is denoted by \mathbf{I}_M . $\text{blkdiag}(\mathbf{X}_1, \dots, \mathbf{X}_N)$ refers to a block diagonal matrix with blocks $\mathbf{X}_1, \dots, \mathbf{X}_N$. $j = \sqrt{-1}$ denotes the imaginary unit. $\mathcal{CN}(\boldsymbol{\mu}, \boldsymbol{\Sigma})$ denotes the complex Gaussian distribution with mean vector $\boldsymbol{\mu}$ and covariance matrix $\boldsymbol{\Sigma}$; \sim means “distributed as”. The first-order partial derivative is denoted by $\dot{\mathbf{f}}(x) = \frac{\partial \mathbf{f}(x)}{\partial x}$. $\mathcal{O}(\cdot)$ represents the standard big-O notation. $\mathbb{E}_X[\cdot]$ stands for the statistical expectation over a random variable X . The Kronecker product is denoted by \otimes . $a \bmod b$ means a modulo b .

II. SYSTEM MODEL

We consider an uplink ISAC system, where a BS equipped with $N \geq 1$ receive antennas aims to sense the location information of an active target equipped with a single antenna and communicate with $K \geq 1$ single-antenna users via the uplink signals sent from the target/users and received at the BS. We focus on a challenging scenario where the direct link between the target and the BS is blocked by obstacles, and a BD-IRS equipped with $M \geq 1$ reflecting elements is deployed to create an additional reflected link for enabling target location sensing and enhancing uplink communication,

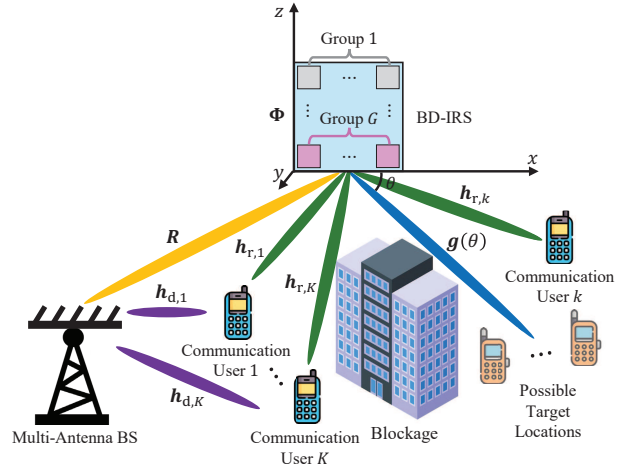


Fig. 1. Illustration of an uplink BD-IRS aided ISAC system with prior distribution information.

as illustrated in Fig. 1. Specifically, we aim to sense the azimuth angle of the target with respect to the BD-IRS denoted by $\theta \in [0, \pi)$, as illustrated in Fig. 1, while the distance between the target and the BD-IRS is assumed to be known as r meters (m).¹ The value of θ is *unknown*, while its PDF denoted by $p_\theta(\theta)$ is known *a priori* at the BS via historic data or target movement pattern [42]–[50].

We consider a general reflective architecture at the BD-IRS, where the M reflecting elements are grouped into G groups, each consisting of M_g elements, with $\sum_{g=1}^G M_g = M$. The elements in each group are inter-connected with a reflecting matrix $\Phi_g \in \mathbb{C}^{M_g \times M_g}$, where $\Phi_g^H \Phi_g = \mathbf{I}_{M_g}$ and $\Phi_g = \Phi_g^T$ hold due to the lossless and reciprocal properties of BD-IRS [20]. The overall BD-IRS reflection matrix is given by

$$\Phi = \text{blkdiag}\{\Phi_1, \dots, \Phi_G\}. \quad (1)$$

Note that when $G = 1$, the above architecture corresponds to a *fully-connected* BD-IRS where inter-connection exists between any two reflecting elements; when $G = M$, the above architecture reduces to a *single-connected* BD-IRS, i.e., conventional IRS, where the BD-IRS reflection matrix becomes a diagonal matrix; while when $1 < G < M$, the above architecture corresponds to a *group-connected* BD-IRS, where inter-group elements are not connected. Moreover, we consider the case where the BD-IRS is located such that the channel from the target to the BD-IRS can be modeled as a line-of-sight (LoS) channel, which is denoted by $\mathbf{g}(\theta) \in \mathbb{C}^{M \times 1}$.² Let M_x and M_z denote the number of reflecting elements in each row and column of the BD-IRS, respectively, with $M_x M_z = M$. Each element in $\mathbf{g}(\theta)$ is thus modeled as [55]³

$$g_m(\theta) = \frac{\beta_0}{r} e^{j \frac{2\pi \Delta}{\lambda} (m-1) \bmod M_x \cos \theta}, \quad m = 1, \dots, M, \quad (2)$$

¹The distance between the target and BD-IRS can be estimated via first estimating the distance from the target to the BS via the BD-IRS using time-of-arrival (ToA) methods (see, e.g., [15], [54]) and then subtracting the known distance between the BS and the BD-IRS, or known *a priori* based on target movement pattern or historic data [42]–[50].

²This is practically feasible with known PDF of the target’s location.

³In this paper, we put all the elements in each group on the same row [56], while our results are also directly applicable to other grouping strategies.

where β_0 denotes the reference channel gain at 1 m, Δ denotes the spacing between adjacent reflecting elements in m, and λ denotes the wavelength in m. Furthermore, let $\mathbf{R} \in \mathbb{C}^{N \times M}$ denote the channel from the BD-IRS to the BS. The effective target-BS channel is thus given by $\mathbf{R}\Phi\mathbf{g}(\theta)$, for which the exact value is unknown due to the unknown θ , while the statistical information can be derived based on the PDF of θ . Let $\mathbf{h}_{r,k} \in \mathbb{C}^{M \times 1}$ denote the channel from user k to the BD-IRS, and $\mathbf{h}_{d,k} \in \mathbb{C}^{N \times 1}$ denote the direct channel from user k to the BS.⁴ The effective channel from each communication user k to the BS is thus given by

$$\mathbf{h}_k(\Phi) = \mathbf{h}_{d,k} + \mathbf{R}\Phi\mathbf{h}_{r,k}, \quad k = 1, \dots, K. \quad (3)$$

Note that the direct communication channels and cascaded communication channels can be estimated via various channel estimation techniques [57]–[59], and are assumed to be perfectly known in this paper.

We focus on ISAC in a block of L symbol intervals during which both the target's location and the wireless channels remain static. Let $\sqrt{P_0}s_l \in \mathbb{C}$ denote the sensing signal sent from the target at each l -th symbol interval, where P_0 denotes the power budget at the target, and s_l denotes the probing signal *known* at the BS. We further assume $|s_l|^2 = 1$, $l = 1, \dots, L$, which yields a sample covariance for sensing of $\frac{1}{L} \sum_{l=1}^L P_0 |s_l|^2 = P_0$.⁵ Let $c_{k,l} \sim \mathcal{CN}(0, 1)$ denote the information symbol for each k -th communication user at the l -th symbol interval, and P_k denote the average transmit power at each k -th communication user. The received signal at the BS in each l -th symbol interval is thus expressed as

$$\mathbf{y}_l = \mathbf{R}\Phi\mathbf{g}(\theta)\sqrt{P_0}s_l + \sum_{k=1}^K \mathbf{h}_k(\Phi)\sqrt{P_k}c_{k,l} + \mathbf{n}_l, \quad l = 1, \dots, L, \quad (4)$$

where $\mathbf{n}_l \sim \mathcal{CN}(\mathbf{0}, \sigma^2 \mathbf{I}_N)$ denotes the circularly symmetric complex Gaussian (CSCG) noise vector at the BS receiver with average noise power σ^2 at each antenna. The collection of the received signals over L symbol intervals denoted by $\mathbf{Y} = [\mathbf{y}_1, \dots, \mathbf{y}_L] \in \mathbb{C}^{N \times L}$ is thus given by

$$\mathbf{Y} = \mathbf{R}\Phi\mathbf{g}(\theta)\sqrt{P_0}\mathbf{s}^T + \sum_{k=1}^K \mathbf{h}_k(\Phi)\sqrt{P_k}\mathbf{c}_k^T + \mathbf{N}, \quad (5)$$

where $\mathbf{s} = [s_1, \dots, s_L]^T \in \mathbb{C}^{L \times 1}$ and $\mathbf{c}_k = [c_{k,1}, \dots, c_{k,L}]^T \in \mathbb{C}^{L \times 1}$ denote the collections of sensing probing signals and information symbols from each user k , respectively; $\mathbf{N} = [\mathbf{n}_1, \dots, \mathbf{n}_L] \in \mathbb{C}^{N \times L}$ denotes the collection of receiver noise. The BS performs sensing of θ based on \mathbf{Y} and $p_\Theta(\theta)$, and detection of the information symbols sent at each l -th symbol interval based on each \mathbf{y}_l .

Specifically, at the BS receiver, linear receive beamforming is adopted for information symbol detection. For each k -th user, denote $\mathbf{w}_k \in \mathbb{C}^{N \times 1}$ as the receive beamforming vector for user k , for which the beamforming output at each symbol interval is given by

$$y_{k,l} = \mathbf{w}_k^H \mathbf{y}_l = \mathbf{w}_k^H \mathbf{h}_k(\Phi)\sqrt{P_k}c_{k,l} + \mathbf{w}_k^H \mathbf{R}\Phi\mathbf{g}(\theta)\sqrt{P_0}s_l$$

⁴Note that this model is also applicable to the case where the user-BS link is blocked for some user(s), by setting the direct channel(s) as zero.

⁵Note that in practice, there are various ways to design the sensing probing signals, e.g., via using the Zadoff-Chu sequence.

$$+ \sum_{\substack{k'=1 \\ k' \neq k}}^K \mathbf{w}_k^H \mathbf{h}_{k'}(\Phi)\sqrt{P_{k'}}c_{k',l} + \mathbf{w}_k^H \mathbf{n}_l, \quad l = 1, \dots, L. \quad (6)$$

Note that besides the interference from other communication users, the uplink signal sent from the sensing target also causes interference to each communication user, which cannot be canceled due to the unknown location of the target and consequently unknown channel $\mathbf{g}(\theta)$ from the target to the BD-IRS. The SINR for each k -th communication user is thus given by

$$\gamma_k(\mathbf{w}_k, \Phi, \theta) = \frac{P_k |\mathbf{w}_k^H \mathbf{h}_k(\Phi)|^2}{\sum_{\substack{k'=1 \\ k' \neq k}}^K P_{k'} |\mathbf{w}_k^H \mathbf{h}_{k'}(\Phi)|^2 + P_0 |\mathbf{w}_k^H \mathbf{R}\Phi\mathbf{g}(\theta)|^2 + \|\mathbf{w}_k\|^2 \sigma^2}, \quad k = 1, \dots, K. \quad (7)$$

Consequently, the achievable rate is given by $R_k(\mathbf{w}_k, \Phi, \theta) = \log_2(1 + \gamma_k(\mathbf{w}_k, \Phi, \theta))$ in bits per second per Hertz (bps/Hz). Notice that the achievable rate for each communication user is determined by the angular location of the target, θ , which is unknown. However, the known PDF of θ can be leveraged to calculate a tractable lower bound of the expected achievable rate over the random target locations, which is given by

$$\begin{aligned} & \mathbb{E}_\theta[R_k(\mathbf{w}_k, \Phi, \theta)] \\ & \geq \log_2 \left(1 + \frac{P_k |\mathbf{w}_k^H \mathbf{h}_k(\Phi)|^2}{\sum_{\substack{k'=1 \\ k' \neq k}}^K P_{k'} |\mathbf{w}_k^H \mathbf{h}_{k'}(\Phi)|^2 + P_0 \|\mathbf{w}_k^H \mathbf{R}\Phi\mathbf{G}^{\frac{1}{2}}\|^2 + \|\mathbf{w}_k\|^2 \sigma^2} \right) \quad (8) \\ & \triangleq \bar{R}_k(\mathbf{w}_k, \Phi), \quad (9) \end{aligned}$$

where $\mathbf{G} \triangleq \mathbb{E}_\theta[\mathbf{g}(\theta)\mathbf{g}^H(\theta)] = \int_0^\pi \mathbf{g}(\theta)\mathbf{g}^H(\theta) d\theta$. Note that the inequality in (8) holds due to the convexity of $R_k(\mathbf{w}_k, \Phi, \theta)$ over $\mathbf{g}(\theta)\mathbf{g}^H(\theta)$ and Jensen's inequality. By noting that $\bar{R}_k(\mathbf{w}_k, \Phi)$ is only dependent on the design variables \mathbf{w}_k 's and Φ , we will adopt it as the communication performance metric in this paper, which serves as a lower bound of the expected achievable rate for each k -th user. Moreover, note that each receive beamforming vector \mathbf{w}_k only affects the expected rate of its corresponding communication user, thus can be individually optimized to maximize $\bar{R}_k(\mathbf{w}_k, \Phi)$. To this end, we have the following proposition.

Proposition 1: The optimal receive beamforming vector for each k -th communication user that maximizes $\bar{R}_k(\mathbf{w}_k, \Phi)$ is given by

$$\mathbf{w}_k^* = \frac{\Sigma_k^{-1}(\Phi)\mathbf{h}_k(\Phi)}{\|\Sigma_k^{-1}(\Phi)\mathbf{h}_k(\Phi)\|}, \quad (10)$$

where $\Sigma_k(\Phi) = \sigma^2 \mathbf{I}_N + \sum_{k'=1, k' \neq k}^K P_{k'} \mathbf{h}_{k'}(\Phi)\mathbf{h}_{k'}^H(\Phi) + P_0 \mathbf{R}\Phi\mathbf{G}\Phi^H \mathbf{R}^H$.

Proof: Please refer to Appendix A. ■

With the optimized \mathbf{w}_k in Proposition 1, $\bar{R}_k(\mathbf{w}_k, \Phi)$ can be expressed as a function of only the BD-IRS reflection matrix Φ , which is given by

$$\bar{R}_k(\Phi) = \log_2(1 + P_k \mathbf{h}_k^H(\Phi)\Sigma_k^{-1}(\Phi)\mathbf{h}_k(\Phi)). \quad (11)$$

Note that the communication performance is critically dependent on the BD-IRS reflection matrix Φ . On the other hand, the design of Φ also affects the sensing performance via the observations at the BS receiver, i.e., \mathbf{Y} . In the following, we will first characterize the sensing performance when both \mathbf{Y} and $p_\Theta(\theta)$ are exploited. Then, we will formulate and study the BD-IRS reflection optimization problem to strike an optimal balance between sensing and communication.

III. SENSING PERFORMANCE CHARACTERIZATION VIA PCRB

Due to the difficulty in explicitly characterizing the MSE, we consider a tractable bound for the MSE as the sensing performance metric in this paper. Specifically, we will characterize the PCRB as a tractable lower bound of the sensing MSE when prior information about the distribution of θ can be exploited, which is tight in the moderate-to-high SNR regime. To this end, we first derive the posterior Fisher information for estimating θ , which is given by $F(\Phi) = F_O(\Phi) + F_P$ [60]. Specifically, $F_O(\Phi)$ represents the Fisher information from the observations in \mathbf{Y} , and F_P represents the Fisher information from the prior distribution information in $p_\Theta(\theta)$. To derive $F_O(\Phi)$, we first define $\mathbf{y} = \text{vec}(\mathbf{Y})$ as follows:

$$\mathbf{y} = \begin{bmatrix} \mathbf{R}\Phi\mathbf{g}(\theta)\sqrt{P_0s_1} \\ \vdots \\ \mathbf{R}\Phi\mathbf{g}(\theta)\sqrt{P_0s_L} \end{bmatrix} + \begin{bmatrix} \sum_{k=1}^K \mathbf{h}_k(\Phi)\sqrt{P_k}c_{k,1} \\ \vdots \\ \sum_{k=1}^K \mathbf{h}_k(\Phi)\sqrt{P_k}c_{k,L} \end{bmatrix} + \begin{bmatrix} \mathbf{n}_1 \\ \vdots \\ \mathbf{n}_L \end{bmatrix}. \quad (12)$$

Note that $\mathbf{y} \sim \mathcal{CN}(\boldsymbol{\mu}(\theta), \mathbf{C}(\theta))$, where $\boldsymbol{\mu}(\theta) = \sqrt{P_0}\mathbf{R}\Phi\mathbf{g}(\theta) \otimes \mathbf{s}$ and $\mathbf{C}(\theta) = \boldsymbol{\Sigma}_0(\Phi) \otimes \mathbf{I}_L$ with $\boldsymbol{\Sigma}_0(\Phi) = \sum_{k=1}^K P_k \mathbf{h}_k(\Phi)\mathbf{h}_k^H(\Phi) + \sigma^2 \mathbf{I}_N$ representing the covariance matrix of interference-plus-noise for sensing. Then, the log-likelihood function for estimating θ from \mathbf{y} is given by

$$\begin{aligned} \ln(f(\mathbf{y}|\theta)) &= 2\sqrt{P_0}\Re\left\{ \sum_{l=1}^L \mathbf{y}_l^H \boldsymbol{\Sigma}_0^{-1}(\Phi) \mathbf{R}\Phi\mathbf{g}(\theta) s_l \right\} \\ &\quad - NL \ln(\pi \det(\boldsymbol{\Sigma}_0(\Phi))) - \sum_{l=1}^L \mathbf{y}_l^H \boldsymbol{\Sigma}_0^{-1}(\Phi) \mathbf{y}_l \\ &\quad - P_0 \sum_{l=1}^L (\mathbf{R}\Phi\mathbf{g}(\theta) s_l)^H \boldsymbol{\Sigma}_0^{-1}(\Phi) \mathbf{R}\Phi\mathbf{g}(\theta) s_l. \end{aligned} \quad (13)$$

$F_O(\Phi)$ can be thus derived as

$$\begin{aligned} F_O(\Phi) &= -\mathbb{E}_{\mathbf{y},\theta} \left[\frac{\partial^2 \ln(f(\mathbf{y}|\theta))}{\partial \theta^2} \right] \\ &= 2P_0 \mathbb{E}_\theta \left[\sum_{l=1}^L (\mathbf{R}\Phi\dot{\mathbf{g}}(\theta) s_l)^H \boldsymbol{\Sigma}_0^{-1}(\Phi) (\mathbf{R}\Phi\dot{\mathbf{g}}(\theta) s_l) \right] \quad (14) \\ &= 2P_0 \sum_{l=1}^L |s_l|^2 \mathbb{E}_\theta \left[(\mathbf{R}\Phi\dot{\mathbf{g}}(\theta))^H \boldsymbol{\Sigma}_0^{-1}(\Phi) (\mathbf{R}\Phi\dot{\mathbf{g}}(\theta)) \right] \quad (15) \\ &= 2P_0 L \mathbb{E}_\theta \left[(\mathbf{R}\Phi\dot{\mathbf{g}}(\theta))^H \boldsymbol{\Sigma}_0^{-1}(\Phi) (\mathbf{R}\Phi\dot{\mathbf{g}}(\theta)) \right], \quad (16) \end{aligned}$$

where $\dot{\mathbf{g}}(\theta)$ represents the derivative of $\mathbf{g}(\theta)$ with its m -th element being $\dot{g}_m(\theta) = -j \frac{2\pi\Delta}{\lambda} ((m-1) \bmod M_x \sin \theta) g_m(\theta)$, $m = 1, \dots, M$.

Note that the expression of $F_O(\Phi)$ has a sophisticated form because of the complex involvement of the BD-IRS reflection matrix Φ . To further simplify the above expression,

we define $\mathbf{U} \triangleq \mathbb{E}_\theta[\dot{\mathbf{g}}(\theta)\dot{\mathbf{g}}^H(\theta)] = \int_0^\pi \dot{\mathbf{g}}(\theta)\dot{\mathbf{g}}^H(\theta) d\theta$ and its eigenvalue decomposition (EVD) as $\mathbf{U} = \sum_{\zeta=1}^R \kappa_\zeta \mathbf{u}_\zeta \mathbf{u}_\zeta^H$ with $R = \text{rank}(\mathbf{U})$ being its rank. Then, a more tractable expression of $F_O(\Phi)$ can be derived as

$$\begin{aligned} F_O(\Phi) &= 2P_0 L \varphi^H \mathbb{E}_\theta \left[((\mathbf{R}^H \boldsymbol{\Sigma}_0^{-1}(\Phi) \mathbf{R})^T \otimes \dot{\mathbf{g}}(\theta)\dot{\mathbf{g}}^H(\theta)) \right] \varphi \quad (17) \\ &= 2P_0 L \varphi^H ((\mathbf{R}^H \boldsymbol{\Sigma}_0^{-1}(\Phi) \mathbf{R})^T \otimes (\mathbb{E}_\theta[\dot{\mathbf{g}}(\theta)\dot{\mathbf{g}}^H(\theta)])) \varphi \quad (18) \\ &= 2P_0 L \varphi^H ((\mathbf{R}^H \boldsymbol{\Sigma}_0^{-1}(\Phi) \mathbf{R})^T \otimes \left(\sum_{\zeta=1}^R \kappa_\zeta \mathbf{u}_\zeta \mathbf{u}_\zeta^H \right)) \varphi \quad (19) \\ &= 2P_0 L \sum_{\zeta=1}^R \kappa_\zeta \varphi^H ((\mathbf{R}^H \boldsymbol{\Sigma}_0^{-1}(\Phi) \mathbf{R})^T \otimes (\mathbf{u}_\zeta \mathbf{u}_\zeta^H)) \varphi \quad (20) \\ &= 2P_0 L \sum_{\zeta=1}^R \kappa_\zeta (\mathbf{R}\Phi \mathbf{u}_\zeta)^H \boldsymbol{\Sigma}_0^{-1}(\Phi) (\mathbf{R}\Phi \mathbf{u}_\zeta), \quad (21) \end{aligned}$$

where $\varphi = \text{vec}(\Phi^H)$, (17) holds due to $\mathbf{a}^H \mathbf{X} \mathbf{B} \mathbf{X}^H \mathbf{c} = \text{vec}^H(\mathbf{X})(\mathbf{B}^T \otimes \mathbf{c} \mathbf{a}^H) \text{vec}(\mathbf{X})$, and (21) holds due to $\text{vec}^H(\mathbf{X})(\mathbf{B}^T \otimes \mathbf{c} \mathbf{a}^H) \text{vec}(\mathbf{X}) = \mathbf{a}^H \mathbf{X} \mathbf{B} \mathbf{X}^H \mathbf{c}$.

On the other hand, the value of F_P can be obtained as follows offline based on $p_\Theta(\theta)$:

$$F_P = -\mathbb{E}_\theta \left[\frac{\partial^2 \ln(p_\Theta(\theta))}{\partial \theta^2} \right] = -\int_{-\infty}^{\infty} \frac{\partial^2 \ln(p_\Theta(\theta))}{\partial \theta^2} p_\Theta(\theta) d\theta. \quad (22)$$

Based on $F_O(\Phi)$ and F_P , the PCRB for the MSE of sensing θ is given by

$$\begin{aligned} \text{PCRB}_\theta(\Phi) &= \frac{1}{F_O(\Phi) + F_P} \quad (23) \\ &= \frac{1}{2P_0 L \sum_{\zeta=1}^R \kappa_\zeta (\mathbf{R}\Phi \mathbf{u}_\zeta)^H \boldsymbol{\Sigma}_0^{-1}(\Phi) (\mathbf{R}\Phi \mathbf{u}_\zeta) + F_P}. \quad (24) \end{aligned}$$

Remark 1 (Practical Example of $p_\Theta(\theta)$): In practice, a typical example of the PDF $p_\Theta(\theta)$ is the Gaussian mixture model, where the realizations of θ tend to concentrate around several highly-probable angles, thus $p_\Theta(\theta)$ is the summation of multiple Gaussian PDFs. Let $\theta_i \in [0, \pi)$, σ_i^2 , and p_i denote the mean, variance, and weight of each i -th Gaussian PDF, $p_\Theta(\theta)$ can be expressed as $p_\Theta(\theta) = \sum_{i=1}^I p_i \frac{1}{\sqrt{2\pi\sigma_i}} e^{-\frac{(\theta-\theta_i)^2}{2\sigma_i^2}}$. In this case, F_P can be derived as $F_P = \sum_{i=1}^I \frac{p_i}{\sigma_i^2} - \int_{-\infty}^{\infty} \frac{\sum_{i_1=1}^I \sum_{i_2=1}^I \eta_{i_1}(\theta) \eta_{i_2}(\theta) (\frac{\theta-\theta_{i_1}}{\sigma_{i_1}^2} - \frac{\theta-\theta_{i_2}}{\sigma_{i_2}^2})^2}{2 \sum_{i=1}^I \eta_i(\theta)} d\theta$, where $\eta_i(\theta) \triangleq p_i \frac{1}{\sqrt{2\pi\sigma_i}} e^{-\frac{(\theta-\theta_i)^2}{2\sigma_i^2}}$ [42]. Note that when the variance of each Gaussian PDF goes to infinity, the Gaussian mixture model is reduced to the uniform distribution model; while when the variance of each Gaussian PDF tends to be zero, the Gaussian mixture model will approach a discrete model.

IV. PROBLEM FORMULATION

In this paper, we aim to optimize the BD-IRS reflection matrix to maximize the minimum (worst-case) expected achievable rate (approximated by its lower bound $\bar{R}_k(\Phi)$) among the multiple communication users, subject to a threshold on the

sensing PCRB denoted by Γ_{PCRB} . The optimization problem is formulated as

$$(P1) \max_{\Phi} \min_{k=1, \dots, K} \log_2(1 + P_k \mathbf{h}_k^H(\Phi) \Sigma_k^{-1}(\Phi) \mathbf{h}_k(\Phi)) \quad (25)$$

$$\text{s.t.} \quad \frac{1}{2P_0 L \sum_{\zeta=1}^R \kappa_{\zeta}(\mathbf{R}\Phi \mathbf{u}_{\zeta})^H \Sigma_0^{-1}(\Phi) (\mathbf{R}\Phi \mathbf{u}_{\zeta}) + F_P} \leq \Gamma_{\text{PCRB}} \quad (26)$$

$$\Phi = \text{blkdiag}\{\Phi_1, \dots, \Phi_G\} \quad (27)$$

$$\Phi_g^H \Phi_g = \mathbf{I}_{M_g}, \quad g = 1, \dots, G \quad (28)$$

$$\Phi_g = \Phi_g^T, \quad g = 1, \dots, G. \quad (29)$$

Note that Problem (P1) is a non-convex optimization problem as the objective function can be shown to be non-concave over Φ , the PCRB can be shown to be a non-convex function over Φ , and the constraints in (28) are non-convex.

Moreover, the optimization of Φ is challenging due to the generally conflicting goals of sensing and communication. For enhancing the communication performance, Φ should be designed to achieve an optimal balance among the multi-user communication rates, while *suppressing* the channel power from the highly-probable target angles to the BD-IRS to mitigate the interference caused by the target. On the other hand, for enhancing the sensing performance, Φ should be designed towards *increasing* the channel power from the highly-probable target angles to the BD-IRS, and mitigating the interference from all communication users via suppressing their channel powers. Note that in downlink mono-static ISAC where the BS performs sensing based on the target-reflected signals, the downlink communication signals contribute to sensing instead of causing interference. The *mutual interference* between communication and sensing in the considered uplink ISAC system thus calls for a new judicious design of the BD-IRS reflection matrix to manage the mutual interference.

Finally, compared with uplink ISAC with conventional diagonal IRS (see, e.g., [17]), the BD-IRS reflection matrix is under more challenging constraints in (27)-(29), under which conventional techniques for simplifying the PCRB/rate expression and handling the optimization problem may not be directly applicable. However, it also provides new design degrees-of-freedom, the full exploitation of which may enable new performance gains.

In the next section, we will propose an efficient algorithm to tackle the non-convexity of (P1) by reformulating it into a more tractable equivalent form and applying PDD framework.

V. PROPOSED SOLUTION TO PROBLEM (P1)

First, by defining $\Gamma \triangleq \frac{\Gamma_{\text{PCRB}} - F_P}{2P_0 L}$ and introducing an auxiliary variable $\alpha > 0$ to represent the minimum SINR among the multiple users, Problem (P1) can be equivalently transformed into the following problem:

$$(P2) \min_{\alpha, \Phi} -\alpha \quad (30)$$

$$\text{s.t.} \quad P_k \mathbf{h}_k^H(\Phi) \Sigma_k^{-1}(\Phi) \mathbf{h}_k(\Phi) \geq \alpha, \quad k = 1, \dots, K \quad (31)$$

$$\sum_{\zeta=1}^R \kappa_{\zeta}(\mathbf{R}\Phi \mathbf{u}_{\zeta})^H \Sigma_0^{-1}(\Phi) (\mathbf{R}\Phi \mathbf{u}_{\zeta}) \geq \Gamma \quad (32)$$

$$\Phi = \text{blkdiag}\{\Phi_1, \dots, \Phi_G\} \quad (33)$$

$$\Phi_g^H \Phi_g = \mathbf{I}_{M_g}, \quad g = 1, \dots, G \quad (34)$$

$$\Phi_g = \Phi_g^T, \quad g = 1, \dots, G. \quad (35)$$

Then, we note that under the unitary constraints in (34), optimization of Φ for balancing the complicated PCRB and rate expressions is very challenging. To resolve this issue, we introduce a set of auxiliary variables $\Psi_g \in \mathbb{C}^{M_g \times M_g}$, $g = 1, \dots, G$, each satisfying $\Psi_g^H \Psi_g = \mathbf{I}_{M_g}$ and $\Phi_g = \Psi_g$. By this means, Problem (P2) and consequently Problem (P1) can be shown to be equivalent to the following problem:

$$(P3) \min_{\alpha, \Phi, \{\Psi_g\}_{g=1}^G} -\alpha \quad (36)$$

$$\text{s.t.} \quad P_k \mathbf{h}_k^H(\Phi) \Sigma_k^{-1}(\Phi) \mathbf{h}_k(\Phi) \geq \alpha, \quad k = 1, \dots, K \quad (37)$$

$$\sum_{\zeta=1}^R \kappa_{\zeta}(\mathbf{R}\Phi \mathbf{u}_{\zeta})^H \Sigma_0^{-1}(\Phi) (\mathbf{R}\Phi \mathbf{u}_{\zeta}) \geq \Gamma \quad (38)$$

$$\Phi = \text{blkdiag}\{\Phi_1, \dots, \Phi_G\} \quad (39)$$

$$\Phi_g = \Phi_g^T, \quad g = 1, \dots, G \quad (40)$$

$$\Phi_g = \Psi_g, \quad g = 1, \dots, G \quad (41)$$

$$\Psi_g^H \Psi_g = \mathbf{I}_{M_g}, \quad g = 1, \dots, G. \quad (42)$$

Note that without the constraints in (41), the optimization of Φ will be more tractable. Motivated by this, we propose a PDD-based algorithm to decouple Φ_g and Ψ_g in (41). Specifically, by transforming the constraints in (41) into a penalty term, the augmented Lagrange (AL) function can be written as

$$\mathcal{L}(\alpha, \{\Phi_g\}_{g=1}^G, \{\Psi_g\}_{g=1}^G, \{\Lambda_g\}_{g=1}^G) \\ = -\alpha + \sum_{g=1}^G \Re\{\text{Tr}(\Lambda_g^H (\Phi_g - \Psi_g))\} + \sum_{g=1}^G \frac{1}{2\rho} \|\Phi_g - \Psi_g\|_{\mathbb{F}}^2, \quad (43)$$

where $\Lambda_g \in \mathbb{C}^{M_g \times M_g}$, $g = 1, \dots, G$ denote the set of dual variables associated with the constraints in (41), and ρ denotes the penalty parameter. Then, we formulate the AL problem as

$$(P4) \min_{\alpha, \Phi, \{\Psi_g\}_{g=1}^G} -\alpha + \sum_{g=1}^G \Re\{\text{Tr}(\Lambda_g^H (\Phi_g - \Psi_g))\} \\ + \sum_{g=1}^G \frac{1}{2\rho} \|\Phi_g - \Psi_g\|_{\mathbb{F}}^2 \quad (44)$$

$$\text{s.t.} \quad P_k \mathbf{h}_k^H(\Phi) \Sigma_k^{-1}(\Phi) \mathbf{h}_k(\Phi) \geq \alpha, \quad k = 1, \dots, K \quad (45)$$

$$\sum_{\zeta=1}^R \kappa_{\zeta}(\mathbf{R}\Phi \mathbf{u}_{\zeta})^H \Sigma_0^{-1}(\Phi) (\mathbf{R}\Phi \mathbf{u}_{\zeta}) \geq \Gamma \quad (46)$$

$$\Phi = \text{blkdiag}\{\Phi_1, \dots, \Phi_G\} \quad (47)$$

$$\Phi_g = \Phi_g^T, \quad g = 1, \dots, G \quad (48)$$

$$\Psi_g^H \Psi_g = \mathbf{I}_{M_g}, \quad g = 1, \dots, G \quad (49)$$

To solve the AL problem, we iteratively optimize Φ and $\{\Psi_g\}_{g=1}^G$ in the inner loop of PDD, while the outer loop selectively updates the dual variables or the penalty parameter. The optimization procedure is given in detail below.

A. (Inner Loop) Optimization of Φ with Given Auxiliary Variables $\{\Psi_g\}_{g=1}^G$

With given $\{\Psi_g\}_{g=1}^G$, (P4) reduces to the following sub-problem:

$$(P4-I) \min_{\alpha, \Phi} -\alpha + \sum_{g=1}^G \Re\{\text{Tr}(\Lambda_g^H(\Phi_g - \Psi_g))\} + \sum_{g=1}^G \frac{1}{2\rho} \|\Phi_g - \Psi_g\|_F^2 \quad (50)$$

$$\text{s.t. } P_k \mathbf{h}_k^H(\Phi) \Sigma_k^{-1}(\Phi) \mathbf{h}_k(\Phi) \geq \alpha, k = 1, \dots, K \quad (51)$$

$$\sum_{\zeta=1}^R \kappa_\zeta (\mathbf{R}\Phi \mathbf{u}_\zeta)^H \Sigma_0^{-1}(\Phi) (\mathbf{R}\Phi \mathbf{u}_\zeta) \geq \Gamma \quad (52)$$

$$\Phi = \text{blkdiag}\{\Phi_1, \dots, \Phi_G\} \quad (53)$$

$$\Phi_g = \Phi_g^T, \quad g = 1, \dots, G. \quad (54)$$

Note that (P4-I) is still a non-convex problem due to the non-convex constraints in (51) and (52). Moreover, the involvement of the inversions of $\Sigma_k(\Phi)$'s and $\Sigma_0(\Phi)$ makes (P4-I) more challenging. To tackle this issue, we transform (P4-I) into an equivalent form in the following proposition.

Proposition 2: Problem (P4-I) is equivalent to the following problem with auxiliary variables $\nu_\zeta \in \mathbb{C}^{N \times 1}, \zeta = 1, \dots, R$ and $\nu_k \in \mathbb{C}^{N \times 1}, k = 1, \dots, K$:

$$(P4-I\text{-eqv}) \min_{\alpha, \Phi, \{\nu_k\}_{k=1}^K, \{\nu_\zeta\}_{\zeta=1}^R} -\alpha + \sum_{g=1}^G \Re\{\text{Tr}(\Lambda_g^H(\Phi_g - \Psi_g))\} + \sum_{g=1}^G \frac{1}{2\rho} \|\Phi_g - \Psi_g\|_F^2 \quad (55)$$

$$\text{s.t. } f_k(\Phi, \nu_k) + \frac{\alpha}{P_k} \leq 0, k = 1, \dots, K \quad (56)$$

$$\sum_{\zeta=1}^R \kappa_\zeta f_\zeta(\Phi, \nu_\zeta) + \Gamma \leq 0 \quad (57)$$

$$\Phi = \text{blkdiag}\{\Phi_1, \dots, \Phi_G\} \quad (58)$$

$$\Phi_g = \Phi_g^T, \quad g = 1, \dots, G, \quad (59)$$

where $f_\zeta(\Phi, \nu_\zeta) \triangleq \nu_\zeta^H \Sigma_0(\Phi) \nu_\zeta - 2\Re\{\nu_\zeta^H \mathbf{R}\Phi \mathbf{u}_\zeta\}$, $\zeta = 1, \dots, R$ and $f_k(\Phi, \nu_k) \triangleq \nu_k^H \Sigma_k(\Phi) \nu_k - 2\Re\{\nu_k^H \mathbf{h}_k\}$, $k = 1, \dots, K$.

Proof: Please refer to Appendix B. \blacksquare

Although Problem (P4-I-eqv) is still non-convex, we propose an alternating optimization algorithm to iteratively optimize (α, Φ) and $(\{\nu_\zeta\}_{\zeta=1}^R, \{\nu_k\}_{k=1}^K)$ as follows.

1) *Optimization of $(\{\nu_\zeta\}_{\zeta=1}^R, \{\nu_k\}_{k=1}^K)$ with Given (α, Φ) :* With given (α, Φ) , the optimal $\{\nu_\zeta\}_{\zeta=1}^R$ and $\{\nu_k\}_{k=1}^K$ can be derived below as shown in the proof of Proposition 2:

$$\nu_\zeta^* = \Sigma_0^{-1}(\Phi) \mathbf{R}\Phi \mathbf{u}_\zeta, \quad \zeta = 1, \dots, R \quad (60)$$

$$\nu_k^* = \Sigma_k^{-1}(\Phi) \mathbf{h}_k(\Phi), \quad k = 1, \dots, K. \quad (61)$$

2) *Optimization of (α, Φ) with Given $(\{\nu_\zeta\}_{\zeta=1}^R, \{\nu_k\}_{k=1}^K)$:* With given $(\{\nu_\zeta\}_{\zeta=1}^R, \{\nu_k\}_{k=1}^K)$, a key difficulty in efficiently optimizing (α, Φ) lies in the complex expression of $f_\zeta(\Phi, \nu_\zeta)$ and $f_k(\Phi, \nu_k)$'s with respect to matrix Φ . Moreover, the large number of optimization variables in Φ also hinders the development of a low-complexity algorithm. This motivates

us to present an equivalent lower-dimension replacement of Φ yielding a more tractable form of $f_\zeta(\Phi, \nu_\zeta)$ and $f_k(\Phi, \nu_k)$'s. Specifically, define $\varphi_g \triangleq \text{vec}(\Phi_g)$, $g = 1, \dots, G$. Then, Φ can be expressed as $\Phi = \text{vec}^{-1}(\sum_{g=1}^G \mathbf{Q}_g \varphi_g)$, where $\mathbf{Q}_g \in \{0, 1\}^{M^2 \times M_g^2}$, $g = 1, \dots, G$ denote a set of indexing matrices given in Appendix C. Furthermore, we reduce the dimension of φ_g 's by exploiting the reciprocal property of Φ . Define $\phi_g \triangleq \text{vech}(\Phi_g) \in \mathbb{C}^{\frac{M_g(M_g+1)}{2} \times 1}$. By introducing a set of duplication matrices $\mathbf{D}_g \in \{0, 1\}^{M_g^2 \times \frac{M_g(M_g+1)}{2}}$, $g = 1, \dots, G$ whose construction is provided in Appendix D, we have $\mathbf{D}_g \phi_g = \varphi_g$, $g = 1, \dots, G$ and consequently $\Phi_g = \text{vec}^{-1}(\mathbf{D}_g \phi_g)$, $g = 1, \dots, G$. The BD-IRS reflection matrix Φ with M^2 elements can be equivalently represented by $\{\phi_g\}_{g=1}^G$ with $\sum_{g=1}^G \frac{M_g(M_g+1)}{2}$ elements as follows:

$$\Phi = \text{vec}^{-1} \left(\sum_{g=1}^G \mathbf{Q}_g \mathbf{D}_g \phi_g \right). \quad (62)$$

As a result, the optimization of $\{\phi_g\}_{g=1}^G$ is equivalent to the optimization of Φ .

Then, we simplify (P4-I-eqv) based on $\{\phi_g\}_{g=1}^G$. To this end, we first expand $f_\zeta(\Phi, \nu_\zeta)$ as

$$f_\zeta(\Phi, \nu_\zeta) = \nu_\zeta^H \Sigma_0(\Phi) \nu_\zeta - 2\Re\{\nu_\zeta^H \mathbf{R}\Phi \mathbf{u}_\zeta\} \quad (63)$$

$$= \sum_{k=1}^K P_k \nu_\zeta^H \mathbf{R}\Phi \mathbf{h}_{r,k} \mathbf{h}_{r,k}^H \Phi^H \mathbf{R}^H \nu_\zeta + \sum_{k=1}^K P_k |\nu_\zeta^H \mathbf{h}_{d,k}|^2 + \sigma^2 \|\nu_\zeta\|^2 + 2 \sum_{k=1}^K P_k \Re\{\nu_\zeta^H \mathbf{R}\Phi \mathbf{h}_{r,k} \mathbf{h}_{d,k}^H \nu_\zeta\} - 2\Re\{\nu_\zeta^H \mathbf{R}\Phi \mathbf{u}_\zeta\}. \quad (64)$$

Based on (62), the first term of (64) can be re-expressed as

$$\sum_{k=1}^K P_k \nu_\zeta^H \mathbf{R}\Phi \mathbf{h}_{r,k} \mathbf{h}_{r,k}^H \Phi^H \mathbf{R}^H \nu_\zeta = \sum_{k=1}^K P_k \text{vec}(\nu_\zeta^H \mathbf{R}\Phi \mathbf{h}_{r,k} \mathbf{h}_{r,k}^H \Phi^H \mathbf{R}^H \nu_\zeta) \quad (65)$$

$$= \sum_{k=1}^K P_k \text{vec}^H(\Phi) \underbrace{(\mathbf{h}_{r,k}^* \mathbf{h}_{r,k}^T \otimes \mathbf{R}^H \nu_\zeta \nu_\zeta^H \mathbf{R})}_{\mathbf{V}_{\zeta,k}} \text{vec}(\Phi) \quad (66)$$

$$= \sum_{k=1}^K P_k \left(\sum_{g=1}^G \mathbf{Q}_g \mathbf{D}_g \phi_g \right)^H \mathbf{V}_{\zeta,k} \left(\sum_{g=1}^G \mathbf{Q}_g \mathbf{D}_g \phi_g \right) \quad (67)$$

$$= \left(\sum_{g=1}^G \mathbf{Q}_g \mathbf{D}_g \phi_g \right)^H \mathbf{V}_\zeta \left(\sum_{g=1}^G \mathbf{Q}_g \mathbf{D}_g \phi_g \right), \quad (68)$$

where (65) holds since $\nu_\zeta^H \mathbf{R}\Phi \mathbf{h}_k \mathbf{h}_k^H(\Phi) \Phi^H \mathbf{R}^H \nu_\zeta$ is a scalar; (66) holds due to $\mathbf{a}^H \mathbf{X} \mathbf{B} \mathbf{X}^H \mathbf{c} = \text{vec}^H(\mathbf{X})(\mathbf{B}^T \otimes \mathbf{c} \mathbf{a}^H) \text{vec}(\mathbf{X})$ and $\mathbf{V}_\zeta = \sum_{k=1}^K P_k \mathbf{V}_{\zeta,k}$. Note that $\mathbf{V}_{\zeta,k}$ is a positive semi-definite (PSD) matrix because it is the Kronecker product of PSD matrices [61]. Thus, \mathbf{V}_ζ is also a PSD matrix. The fourth term of (64) can be re-expressed as

$$2 \sum_{k=1}^K P_k \Re\{\nu_\zeta^H \mathbf{R}\Phi \mathbf{h}_{r,k} \mathbf{h}_{d,k}^H \nu_\zeta\} = 2 \sum_{k=1}^K P_k \Re\{\text{Tr}(\mathbf{h}_{r,k} \mathbf{h}_{d,k}^H \nu_\zeta \nu_\zeta^H \mathbf{R}\Phi)\} \quad (69)$$

$$= 2 \sum_{k=1}^K P_k \Re \left\{ \text{vec}^H(\mathbf{R}^H \boldsymbol{\nu}_\zeta \boldsymbol{\nu}_\zeta^H \mathbf{h}_{d,k} \mathbf{h}_{r,k}^H) \left(\sum_{g=1}^G \mathbf{Q}_g \mathbf{D}_g \phi_g \right) \right\}, \quad (70)$$

which holds due to $\text{Tr}(\mathbf{A}^H \mathbf{B}) = \text{vec}^H(\mathbf{A}) \text{vec}(\mathbf{B})$. Finally, the last term of (64) can be re-expressed as

$$- 2 \Re \left\{ \boldsymbol{\nu}_\zeta^H \mathbf{R} \Phi \mathbf{u}_\zeta \right\} = - 2 \Re \left\{ \text{Tr}(\mathbf{u}_\zeta \boldsymbol{\nu}_\zeta^H \mathbf{R} \Phi) \right\} \quad (71)$$

$$= - 2 \Re \left\{ \text{vec}^H(\mathbf{R}^H \boldsymbol{\nu}_\zeta \mathbf{u}_\zeta^H) \left(\sum_{g=1}^G \mathbf{Q}_g \mathbf{D}_g \phi_g \right) \right\}, \quad (72)$$

which holds due to $\text{Tr}(\mathbf{A}^H \mathbf{B}) = \text{vec}^H(\mathbf{A}) \text{vec}(\mathbf{B})$.

Consequently, $f_\zeta(\Phi, \boldsymbol{\nu}_\zeta)$ can be re-expressed as

$$f_\zeta(\{\phi_g\}_{g=1}^G, \boldsymbol{\nu}_\zeta) = \left(\sum_{g=1}^G \mathbf{Q}_g \mathbf{D}_g \phi_g \right)^H \mathbf{V}_\zeta \left(\sum_{g=1}^G \mathbf{Q}_g \mathbf{D}_g \phi_g \right) - 2 \Re \left\{ \mathbf{q}_\zeta^H \left(\sum_{g=1}^G \mathbf{Q}_g \mathbf{D}_g \phi_g \right) \right\} + \sum_{k=1}^K P_k |\boldsymbol{\nu}_\zeta^H \mathbf{h}_{d,k}|^2 + \sigma^2 \|\boldsymbol{\nu}_\zeta\|^2, \quad (73)$$

where $\mathbf{q}_\zeta^H \triangleq \text{vec}^H(\mathbf{R}^H \boldsymbol{\nu}_\zeta (\mathbf{u}_\zeta^H - \sum_{k=1}^K P_k \boldsymbol{\nu}_\zeta^H \mathbf{h}_{d,k} \mathbf{h}_{r,k}^H))$. Similarly, $f_k(\Phi, \boldsymbol{\nu}_k)$ can be re-expressed as

$$f_k(\{\phi_g\}_{g=1}^G, \boldsymbol{\nu}_k) = \left(\sum_{g=1}^G \mathbf{Q}_g \mathbf{D}_g \phi_g \right)^H \mathbf{J}_k \left(\sum_{g=1}^G \mathbf{Q}_g \mathbf{D}_g \phi_g \right) + \sigma^2 \|\boldsymbol{\nu}_k\|^2 - 2 \Re \left\{ \mathbf{r}_k^H \left(\sum_{g=1}^G \mathbf{Q}_g \mathbf{D}_g \phi_g \right) + \boldsymbol{\nu}_k^H \mathbf{h}_{d,k} \right\} + \sum_{\substack{k'=1 \\ k' \neq k}}^K P_{k'} |\boldsymbol{\nu}_k^H \mathbf{h}_{d,k'}|^2, \quad (74)$$

where $\mathbf{J}_k \triangleq \sum_{k'=1, k' \neq k}^K P_{k'} \mathbf{J}_{k,k'} + P_0 \mathbf{G}^T \otimes (\mathbf{R}^H \boldsymbol{\nu}_k \boldsymbol{\nu}_k^H \mathbf{R})$, $\mathbf{J}_{k,k'} \triangleq (\mathbf{h}_{r,k'}^* \mathbf{h}_{r,k'}^T) \otimes (\mathbf{R}^H \boldsymbol{\nu}_k \boldsymbol{\nu}_k^H \mathbf{R})$, and $\mathbf{r}_k^H \triangleq \text{vec}^H(\mathbf{R}^H \boldsymbol{\nu}_k (\mathbf{h}_{r,k}^H - \sum_{k'=1, k' \neq k}^K P_{k'} \boldsymbol{\nu}_k^H \mathbf{h}_{d,k'} \mathbf{h}_{r,k'}^H))$, $k = 1, \dots, K$. Note that \mathbf{J}_k 's are also PSD matrices. In addition, the objective function of Problem (P4-I-eqv) can be re-expressed as $-\alpha + \sum_{g=1}^G \Re \left\{ \text{Tr}(\boldsymbol{\Lambda}_g^H (\Phi_g - \Psi_g)) \right\} + \sum_{g=1}^G \frac{1}{2\rho} \|\Phi_g - \Psi_g\|_F^2 = -\alpha + \sum_{g=1}^G \Re \left\{ \text{vec}^H(\boldsymbol{\Lambda}_g) (\mathbf{D}_g \phi_g - \text{vec}(\Psi_g)) \right\} + \sum_{g=1}^G \frac{1}{2\rho} \|\mathbf{D}_g \phi_g - \text{vec}(\Psi_g)\|^2$ due to $\text{Tr}(\mathbf{A}^H \mathbf{B}) = \text{vec}^H(\mathbf{A}) \text{vec}(\mathbf{B})$.

Therefore, with given $(\{\boldsymbol{\nu}_\zeta\}_{\zeta=1}^R, \{\boldsymbol{\nu}_k\}_{k=1}^K)$, (α, Φ) can be optimized by solving the following problem on $(\alpha, \{\phi_g\}_{g=1}^G)$ and obtaining the optimal Φ via (62):

(P4-I-eqv')

$$\min_{\alpha, \{\phi_g\}_{g=1}^G} -\alpha + \sum_{g=1}^G \Re \left\{ \text{vec}^H(\boldsymbol{\Lambda}_g) (\mathbf{D}_g \phi_g - \text{vec}(\Psi_g)) \right\} + \sum_{g=1}^G \frac{1}{2\rho} \|\mathbf{D}_g \phi_g - \text{vec}(\Psi_g)\|^2 \quad (75)$$

$$\text{s.t.} \quad \left(\sum_{g=1}^G \mathbf{Q}_g \mathbf{D}_g \phi_g \right)^H \mathbf{J}_k \left(\sum_{g=1}^G \mathbf{Q}_g \mathbf{D}_g \phi_g \right) + \sigma^2 \|\boldsymbol{\nu}_k\|^2 - 2 \Re \left\{ \mathbf{r}_k^H \left(\sum_{g=1}^G \mathbf{Q}_g \mathbf{D}_g \phi_g \right) + \boldsymbol{\nu}_k^H \mathbf{h}_{d,k} \right\} + \sum_{\substack{k'=1 \\ k' \neq k}}^K P_{k'} |\boldsymbol{\nu}_k^H \mathbf{h}_{d,k'}|^2 + \frac{\alpha}{P_k} \leq 0, \quad k = 1, \dots, K \quad (76)$$

$$\sum_{\zeta=1}^R \kappa_\zeta \left\{ \left(\sum_{g=1}^G \mathbf{Q}_g \mathbf{D}_g \phi_g \right)^H \mathbf{V}_\zeta \left(\sum_{g=1}^G \mathbf{Q}_g \mathbf{D}_g \phi_g \right) - 2 \Re \left\{ \mathbf{q}_\zeta^H \left(\sum_{g=1}^G \mathbf{Q}_g \mathbf{D}_g \phi_g \right) \right\} + \sigma^2 \|\boldsymbol{\nu}_\zeta\|^2 + \sum_{k=1}^K P_k |\boldsymbol{\nu}_\zeta^H \mathbf{h}_{d,k}|^2 \right\} + \Gamma \leq 0. \quad (77)$$

By noting \mathbf{J}_k 's and \mathbf{V}_ζ are PSD matrices, (P4-I-eqv') can be shown to be a convex second-order cone program (SOCP), for which the optimal solution can be obtained via the interior-point method [62] or existing software such as CVX [63].

3) *Overall Algorithm for Problem (P4-I-eqv)*: To summarize, the optimal solutions to (α, Φ) and $(\{\boldsymbol{\nu}_\zeta\}_{\zeta=1}^R, \{\boldsymbol{\nu}_k\}_{k=1}^K)$ can be iteratively obtained with the other being fixed at each time. Since the objective value of Problem (P4-I-eqv) is bounded below, monotonic convergence is guaranteed for this alternating optimization algorithm.

B. (Inner Loop) Optimization of Auxiliary Variables $\{\Psi_g\}_{g=1}^G$ with Given Φ

Note that $\Re \left\{ \text{Tr}(\boldsymbol{\Lambda}_g^H (\Phi_g - \Psi_g)) \right\} + \frac{1}{2\rho} \|\Phi_g - \Psi_g\|_F^2 = \frac{1}{2\rho} (\|\Psi_g - (\Phi_g + \rho \boldsymbol{\Lambda}_g)\|_F^2 - \rho^2 \text{Tr}(\boldsymbol{\Lambda}_g^H \boldsymbol{\Lambda}_g))$ holds. Thus, with given Φ , the sub-problem for optimizing Ψ_g is given by

$$(P4-II) \quad \min_{\Psi_g} \|\Psi_g - (\Phi_g + \rho \boldsymbol{\Lambda}_g)\|_F^2 \quad (78)$$

$$\text{s.t.} \quad \Psi_g^H \Psi_g = \mathbf{I}_{M_g}. \quad (79)$$

Denote $\Phi_g + \rho \boldsymbol{\Lambda}_g = \tilde{\mathbf{U}}_g \tilde{\mathbf{S}}_g \tilde{\mathbf{V}}_g^H$ as the singular value decomposition (SVD) of $\Phi_g + \rho \boldsymbol{\Lambda}_g$. Note that the objective function of (P4-II) is convex, while the only constraint is a unitary constraint. According to [64], the optimal solution to (P4-II) can be derived in closed form as

$$\Psi_g^* = \tilde{\mathbf{U}}_g \tilde{\mathbf{V}}_g^H. \quad (80)$$

C. (Outer Loop) Update of Dual Variables $\{\boldsymbol{\Lambda}_g\}_{g=1}^G$ or Penalty Parameter ρ

In each outer iteration, we only update either the dual variables $\{\boldsymbol{\Lambda}_g\}_{g=1}^G$ or the penalty parameter ρ based on a predefined constraint violation level ϵ [53]. If the equality constraints in (41) are approximately satisfied with a violation lower than ϵ , i.e., $\|\Phi_g - \Psi_g\|_\infty \leq \epsilon$, $g = 1, \dots, G$, each dual variable $\boldsymbol{\Lambda}_g$ is updated as

$$\boldsymbol{\Lambda}_g \leftarrow \boldsymbol{\Lambda}_g + \frac{1}{\rho} (\Phi_g - \Psi_g). \quad (81)$$

Otherwise, ρ is decreased as follows to enhance the penalty term to push the equality constraint towards being satisfied:

$$\rho \leftarrow \delta \rho, \quad (82)$$

where $0 < \delta < 1$ is the shrinkage factor.

TABLE I
COMPLEXITY ANALYSIS FOR PROPOSED PDD-BASED ALGORITHM FOR
PROBLEM (P1)

Optimization Part	Complexity
$\{\nu_\zeta\}_{\zeta=1}^R, \{\nu_k\}_{k=1}^K$	$\mathcal{O}(N^3)$
(α, Φ)	$\mathcal{O}(K^{1.5}(\sum_{g=1}^G M_g^2)^3)$
$\{\Psi_g\}_{g=1}^G$	$\sum_{g=1}^G M_g^3$
Problem (P1)	$\mathcal{O}(L_P L_O L_I L_{P4} (N^3 + K^{1.5}(\sum_{g=1}^G M_g^2)^3))$

D. Overall PDD-based Algorithm for Problem (P1)

To summarize, the overall PDD-based algorithm for (P4) consists of two loops. In the outer loop, the dual variables in $\{\Lambda_g\}_{g=1}^G$ or the penalty parameter ρ is updated based on the constraint violation level of (41) according to (81) and (82). In the inner loop, the optimal solutions to (α, Φ) , auxiliary vectors $(\{\nu_\zeta\}_{\zeta=1}^R, \{\nu_k\}_{k=1}^K)$, and auxiliary matrices $\{\Psi_g\}_{g=1}^G$ are iteratively obtained by solving the convex problem (P4-I-eqv') and recovering Φ via (62) or according to the closed-form expressions in (60), (61), and (80), respectively. Note that as the optimal solution to each sub-problem is obtained in each step, convergence can be achieved for the proposed PDD-based algorithm, which will be verified in Section VII. By updating the penalty parameter ρ , the constraint violation level can be controlled under the given threshold ϵ . Moreover, to further enhance the performance, the above procedure can be repeated for $L_P > 1$ times with different initialization, among which the best solution can be selected, while we will present one initialization method in Section V-E. Finally, the obtained solution of Φ for (P4) automatically serves as a high-quality suboptimal solution to (P1). Let L_O and L_I denote the numbers of outer and inner loops in the proposed algorithm. Let L_{P4} denote the iteration numbers for solving (P4-I-eqv). The overall complexity of the proposed algorithm is analyzed in Table I, which is observed to be polynomial over key system parameters N , K , and M_g 's.

E. Extension to BD-IRS Aided Uplink Sensing for PCRB Minimization

Finally, we note that the proposed algorithm can be extended to deal with the PCRB minimization problem in a BD-IRS aided uplink sensing system, where no communication user is present. The problem is formulated as

$$(P5) \min_{\Phi} \frac{1}{2P_0 L \sum_{\zeta=1}^R \kappa_\zeta(\mathbf{R}\Phi\mathbf{u}_\zeta)^H \Sigma_0^{-1}(\Phi)(\mathbf{R}\Phi\mathbf{u}_\zeta) + F_P} \quad (83)$$

$$\text{s.t. } \Phi = \text{blkdiag}\{\Phi_1, \dots, \Phi_G\} \quad (84)$$

$$\Phi_g^H \Phi_g = \mathbf{I}_{M_g}, \quad g = 1, \dots, G \quad (85)$$

$$\Phi_g = \Phi_g^T, \quad g = 1, \dots, G. \quad (86)$$

Notice that the objective PCRB function of (P5) appears in the constraints of (P2). Thus, by introducing auxiliary variables Ψ_g 's and ν_ζ 's, we can formulate the AL problem for (P5) under the PDD framework and obtain a high-quality solution to (P5) in a similar manner, for which the details are omitted due to limited space. Note that the solution to (P5) can serve as an initial point for the proposed algorithm for (P1), as it aims to achieve the minimum PCRB value and consequently satisfy the PCRB constraint in (26).

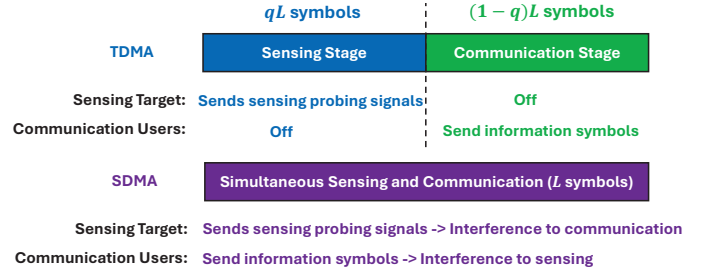


Fig. 2. Comparison between the SDMA scheme and TDMA scheme.

VI. BD-IRS AIDED UPLINK ISAC UNDER TDMA

In the previous sections, we studied an SDMA scheme where the interference between sensing and communication is managed via BD-IRS reflection and BS receive beamforming optimization. However, the new mutual interference between sensing and communication is more severe than the one-way interference from sensing to communication in mono-static downlink ISAC. Particularly, as BD-IRS has a constrained circuit architecture, its effectiveness in simultaneously two conflicting goals in sensing and communication is generally limited. This thus motivates us to explore whether other strictly orthogonal multiple access schemes can achieve enhanced performance via removing such mutual interference.

In this section, we propose a TDMA scheme for uplink BD-IRS aided ISAC illustrated in Fig. 2, where the sensing target sends uplink signals for sensing during qL symbol intervals (i.e., the *sensing stage*), where $q \in [0, 1]$ denotes the fraction of time for sensing, while the K communication users send uplink signals during the other $(1-q)L$ symbol intervals (i.e., the *communication stage*). In this case, two different BD-IRS reflection matrices denoted by Φ_S and Φ_C can be separately designed to optimize the sensing PCRB and minimum communication user rate, and implemented in the sensing stage and communication stage, respectively.

During the sensing stage, the interference from communication users is not present, and the interference-plus-noise covariance matrix reduces to the noise covariance matrix $\Sigma_0(\Phi_S) = \sigma^2 \mathbf{I}_N$. Thus, the PCRB expression is given by $\text{PCRB}^{\text{TDMA}}(\Phi_S) = \frac{1}{\frac{2P_0 q L}{\sigma^2} \sum_{\zeta=1}^R \kappa_\zeta(\mathbf{R}\Phi_S \mathbf{u}_\zeta)^H (\mathbf{R}\Phi_S \mathbf{u}_\zeta) + F_P}$. Then, Φ_S can be optimized to minimize $\text{PCRB}^{\text{TDMA}}(\Phi_S)$ using a similar method as in Section V-E.

During the communication stage, the SINR given below is no longer a random variable as the sensing-generated interference due to the randomly located target is not present:

$$\gamma_k^C(\mathbf{w}_k, \Phi_C) = \frac{P_k |\mathbf{w}_k^H \mathbf{h}_k(\Phi_C)|^2}{\sum_{\substack{k'=1 \\ k' \neq k}}^K P_{k'} |\mathbf{w}_k^H \mathbf{h}_{k'}(\Phi_C)|^2 + \sigma^2 \|\mathbf{w}_k\|^2} \quad (87)$$

$$= \frac{P_k |\mathbf{w}_k^H \mathbf{h}_k(\Phi_C)|^2}{\mathbf{w}_k^H \Sigma_k^C(\Phi_C) \mathbf{w}_k}, \quad (88)$$

where $\Sigma_k^C(\Phi_C) = \sum_{k'=1, k' \neq k}^K P_{k'} \mathbf{h}_{k'}(\Phi_C) \mathbf{h}_{k'}^H(\Phi_C) + \sigma^2 \mathbf{I}_N$, $k = 1, \dots, K$. Given optimal $\mathbf{w}_k^* = \frac{\Sigma_k^C(\Phi_C) \mathbf{h}_k(\Phi_C)}{\|\Sigma_k^C(\Phi_C) \mathbf{h}_k(\Phi_C)\|}$,

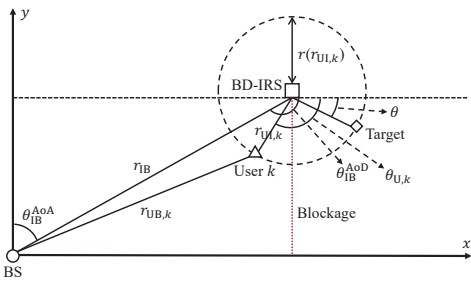


Fig. 3. Topology of the BD-IRS aided uplink ISAC system.

the effective achievable rate is expressed as follows in bps/Hz:

$$R_k^{\text{TDMA}}(\Phi_C) = (1-q) \log_2(1 + P_k \mathbf{h}_k^H(\Phi_C) \Sigma_k^{C-1}(\Phi_C) \mathbf{h}_k(\Phi_C)). \quad (89)$$

Then, Φ_C can be designed to maximize the minimum rate among $R_k^{\text{TDMA}}(\Phi_C)$'s, which can be done via a similar PDD-based algorithm as in Section V.

Note that increasing the time allocated to sensing (i.e., increasing q) will reduce the PCRB, but also leads to smaller communication rates. The optimal TDMA time allocation can be obtained via solving the following problem:

$$\begin{aligned} \text{(P6)} \quad & \max_{q \in [0,1]} \min_{k=1, \dots, K} (1-q) \log_2 \left(1 + \right. \\ & \left. \frac{P_k \mathbf{h}_k^H(\Phi_C) \Sigma_k^{C-1}(\Phi_C) \mathbf{h}_k(\Phi_C)}{1} \right) \quad (90) \\ \text{s.t.} \quad & \frac{\frac{2P_0 q L}{\sigma^2} \sum_{\zeta=1}^R \kappa_{\zeta} (\mathbf{R} \Phi_S \mathbf{u}_{\zeta})^H (\mathbf{R} \Phi_S \mathbf{u}_{\zeta}) + F_P}{1} \leq \Gamma_{\text{PCRB}}. \quad (91) \end{aligned}$$

Note that both the objective function to be maximized and the left-hand-side of the constraint in (91) are non-increasing functions of q . Thus, (P6) is feasible if and only if

$$\frac{1}{\frac{2P_0 q L}{\sigma^2} \sum_{\zeta=1}^R \kappa_{\zeta} (\mathbf{R} \Phi_S \mathbf{u}_{\zeta})^H (\mathbf{R} \Phi_S \mathbf{u}_{\zeta}) + F_P} \leq \Gamma_{\text{PCRB}}$$

holds, and its optimal solution is given by⁶

$$q^* = \max \left\{ \frac{\frac{1}{\Gamma_{\text{PCRB}}} - F_P}{\frac{2P_0 L}{\sigma^2} \sum_{\zeta=1}^R \kappa_{\zeta} (\mathbf{R} \Phi_S \mathbf{u}_{\zeta})^H (\mathbf{R} \Phi_S \mathbf{u}_{\zeta})}, 0 \right\}. \quad (92)$$

Note that although a pre-log factor $1-q$ is applied in the achievable rate, the removal of interference in both $\Sigma_k^C(\Phi_C)$'s and $\Sigma_0(\Phi_S)$ as well as the separate tailored design of BD-IRS reflection matrix in the two stages also bring new benefits. In the next section, we will compare the performance of TDMA versus SDMA to draw more useful insights.

VII. NUMERICAL RESULTS

In this section, we provide numerical results to evaluate the effectiveness of our proposed BD-IRS reflection matrix design. Under a two-dimensional Cartesian coordinate system, the topology of the system is illustrated in Fig. 3, where the distance between the BD-IRS and the BS is set as $r_{\text{IB}} = 200$

⁶The obtained number of symbol intervals can be rounded up to the nearest integer if needed.

m, the distance between the possible locations of the target as well as the communication users and the BD-IRS is set as $r = r_{\text{UI},k} = 10$ m, $k = 1, \dots, K$. The BS is equipped with a uniform linear array (ULA) vertical to the x -axis, while the BD-IRS lies on the $x-z$ plane. The spacings between adjacent BS antennas and BD-IRS elements are set as $\Delta = \frac{\lambda}{2}$. Let $\theta_{U,k}$ denote the angle-of-arrival (AoA) from each k -th user to the BD-IRS. Let $\theta_{\text{IB}}^{\text{AoA}} = \frac{\pi}{4}$ and $\theta_{\text{IB}}^{\text{AoD}} = \theta_{\text{IB}}^{\text{AoA}} + \frac{\pi}{2}$ denote the AoA and angle-of-departure (AoD) of the link from the BD-IRS to the BS, respectively. Then, the distance between each k -th user and the BS can be calculated as $r_{\text{UB},k} = \sqrt{r_{\text{IB}}^2 + r_{\text{UI},k}^2 - 2r_{\text{IB}}r_{\text{UI},k} \cos(\theta_{\text{IB}}^{\text{AoD}} - \theta_{U,k})}$. We consider a Rician fading model for the channel from the BD-IRS to the BS with $\mathbf{R} = \beta_{\text{IB}} \sqrt{\frac{1}{\chi+1}} (\sqrt{\chi} \mathbf{H}_{\text{LoS}} + \mathbf{H}_{\text{NLoS}})$, where $\chi = -8$ dB is the Rician factor, β_{IB} denotes the path gain given by $\beta_{\text{IB}} = \frac{\beta_0}{r_{\text{IB}}}$ with $\beta_0 = -33$ dB, \mathbf{H}_{LoS} represents the LoS component, and \mathbf{H}_{NLoS} represents the non-LoS (NLoS) component following Rayleigh fading, respectively. The LoS component can be expressed as $\mathbf{H}_{\text{LoS}} = \mathbf{a}(\theta_{\text{IB}}^{\text{AoA}}) \mathbf{b}^H(\theta_{\text{IB}}^{\text{AoD}})$, where $a_n(\theta_{\text{IB}}^{\text{AoA}}) = e^{j\pi(n-1) \cos \theta_{\text{IB}}^{\text{AoA}}}$, $n = 1, \dots, N$ and $b_m(\theta_{\text{IB}}^{\text{AoD}}) = e^{j\pi(m-1) \bmod M_x \cos \theta_{\text{IB}}^{\text{AoD}}}$, $m = 1, \dots, M$ are steering vectors at the BS and the BD-IRS, respectively. We consider a Rayleigh fading model for the channels from the users to the BS with path loss exponent 3.5, and consider an LoS model for the channels from the users to the BD-IRS with $h_{r,k,m}(\theta_{U,k}) = \frac{\beta_0}{r_{\text{UI},k}} e^{j\pi(m-1) \bmod M_x \cos \theta_{U,k}}$, $m = 1, \dots, M$.

We consider $K = 2$ communication users, $N = 16$ receive antennas at the BS, $P_0 = P_1 = P_2 = 10$ dBm, $\sigma^2 = -95$ dBm, $L = 25$, and $M_x = M_z = 4$ if not specified otherwise. The azimuth angles of users are set as $\theta_{U,1} = \frac{5\pi}{9}$ and $\theta_{U,2} = \frac{7\pi}{9}$. The PDF of θ is assumed to follow the Gaussian mixture model in Remark 1 with $p_1 = 0.31$, $\theta_1 = \frac{5\pi}{18}$, $\sigma_1^2 = 10^{-3}$, $p_2 = 0.43$, $\theta_2 = \frac{11\pi}{36}$, $\sigma_2^2 = 10^{-3}$, and $p_3 = 0.26$, $\theta_3 = \frac{\pi}{3}$, $\sigma_3^2 = 10^{-3}$. We set $\Gamma_{\text{PCRB}} = 5 \times 10^{-4}$ and consider the fully-connected case unless otherwise specified.

For comparison with the proposed design, we consider the following two benchmark schemes:

- **Benchmark Scheme 1: Isotropic reflection.** We set $\Phi = \mathbf{I}_M$ which corresponds to isotropic reflection and can also be realized using conventional diagonal IRS.
- **Benchmark Scheme 2: Random reflection.** We randomly generate 100 BD-IRS reflection matrices under the fully-connected architecture, and select the best one among them.

A. Convergence Behavior of Proposed PDD-based Algorithms

First, Fig. 4(a) and Fig. 4(b) show the convergence behavior of the proposed PDD-based algorithms for the PCRB minimization problem in (P5) and the minimum rate maximization problem in (P1), where monotonic and quick convergence (within 10 and 20 iterations) is observed for both problems. This validates the effectiveness of the PDD-based algorithms.

B. Evaluation of Sensing Performance Aided by BD-IRS

In this subsection, we evaluate the performance of sensing in terms of PCRB with the aid of BD-IRS when no communication user is present. Fig. 5(a) and Fig. 5(b) show the

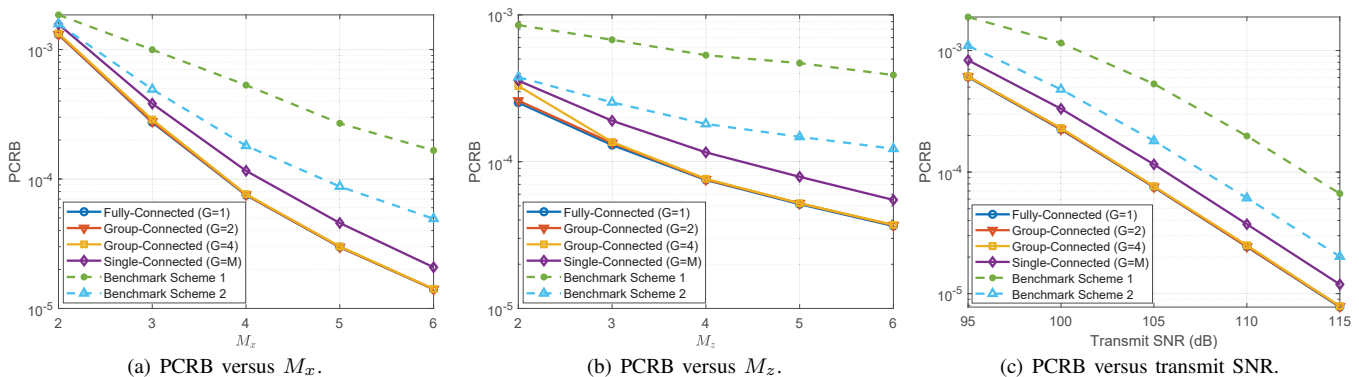


Fig. 5. PCRB versus M_x/M_z /transmit SNR for BD-IRS aided sensing.

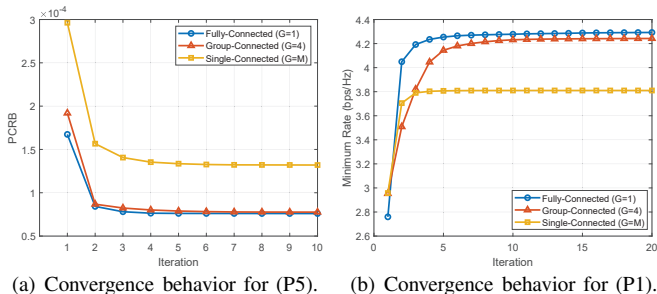


Fig. 4. Convergence behavior of the proposed PDD-based algorithms for sensing-only and ISAC systems.

PCRb versus the number of reflecting elements in the x -axis and z -axis (i.e., M_x and M_z) with the other one fixed as 4, respectively. Fig. 5(c) shows the PCRb versus transmit SNR $\frac{P_0}{\sigma^2} = \frac{P_1}{\sigma^2} = \frac{P_2}{\sigma^2}$. It is observed from that the PCRb decreases as M_x , M_z , or transmit SNR increases; moreover, the fully-connected and group-connected architectures outperform the single-connected architecture (i.e., conventional diagonal IRS) as well as the two benchmark schemes, where the performance gain of BD-IRS over diagonal IRS enlarges as M_x or M_z increases. Additionally, it is observed that increasing M_x is more effective in lowering the PCRb compared with increasing M_z , since the increment in M_x can provide additional sensing information on θ , which can be drawn from $\dot{\mathbf{g}}(\theta)$ in the PCRb expression, while increasing M_z can mainly enhance the overall target-BS effective channel gain (or aperture gain).

C. Evaluation of ISAC Performance Aided by BD-IRS

Next, we evaluate the performance of ISAC aided by BD-IRS. In Fig. 6(a), we show the minimum rate versus the PCRb threshold Γ_{PCRb} . Benchmark schemes and the single-connected IRS are not shown for comparison as they may not always yield a feasible solution to Problem (P1). The results indicate that the minimum rate achieved by the proposed design increases as Γ_{PCRb} increases, which validates the trade-off between sensing and communication. Moreover, the TDMA scheme is generally outperformed by the SDMA scheme, due to the excessive time waste resulting from orthogonal signal transmission. Then, we set $\Gamma_{\text{PCRb}} = 1.5 \times 10^{-3}$ and show the minimum rate versus M_z in Fig. 6(b). It can be observed that the minimum rate increases as M_z increases, and the proposed design outperforms both benchmark schemes by a large margin. Furthermore, it is observed that as the number of groups decreases, the performance improves at a

TABLE II
PERFORMANCE AND COMPLEXITY COMPARISON OF FULLY-, GROUP-, AND SINGLE-CONNECTED BD-IRSS ($M_x = M_z = 4$).

Architecture	Fully-	Group-	Single-	
Group Number	1	2	4	M
Circuit Topology Complexity	$\frac{M(M+1)}{2}$	$\frac{M(M/2+1)}{2}$	$\frac{M(M/4+1)}{2}$	M
Optimization Computational Complexity	$\mathcal{O}(K^{1.5}M^6)$	$\mathcal{O}(\frac{K^{1.5}M^6}{8})$	$\mathcal{O}(\frac{K^{1.5}M^6}{64})$	$\mathcal{O}(K^{1.5}M^3)$
PCRb ($\times 10^{-5}$)	7.506	7.560	7.642	11.573
Performance Gain (PCRb)	35.142%	34.680%	33.968%	
Minimum Rate	4.078	4.044	3.963	3.646
Performance Gain (Minimum Rate)	11.852%	10.912%	8.687%	

cost of a more complicated architecture, which is summarized in Table II. In addition, it is also noted that BD-IRS can use less elements to achieve the same performance as conventional IRS, which is helpful to reduce the hardware cost and physical size. For instance, in Fig. 6(b), BD-IRS with 2 groups and $M_z = 4$ can achieve comparable performance as conventional IRS with $M_z = 6$. In Fig. 6(c), we show the minimum rate versus transmit SNR with $\Gamma_{\text{PCRb}} = 2.2 \times 10^{-3}$. It is observed that the minimum rate increases as the transmit SNR increases. On the other hand, we show the effective sensing signal power in Fig. 7, which is defined as the effective sensing signal power received at the BS from a location at distance 10 m and angle θ with respect to the BD-IRS via reflection of the BD-IRS, i.e., $P_0 |\mathbf{w}_0^H \mathbf{R} \Phi \mathbf{g}(\theta)|^2$, where $\mathbf{w}_0 \in \mathbb{C}^{N \times 1}$ denotes an auxiliary receive beamforming vector at the BS for the sensing signal.⁷ Motivated by the relationship between the sensing SINR and the PCRb, \mathbf{w}_0 is designed to maximize the expected sensing SINR given by

$$\begin{aligned} \bar{\gamma}_s(\mathbf{w}_0, \Phi) &\triangleq \mathbb{E}_\theta[\gamma_s(\mathbf{w}_0, \Phi, \theta)] \\ &= \frac{P_0 \mathbf{w}_0^H \mathbb{E}_\theta[\mathbf{R} \Phi \mathbf{g}(\theta) \mathbf{g}^H(\theta) \Phi^H \mathbf{R}^H] \mathbf{w}_0}{\mathbf{w}_0^H \Sigma_0 \mathbf{w}_0}, \quad (93) \end{aligned}$$

⁷Note that the PCRb derived in this paper can bound the MSE with any receive signal processing and estimation method, while we consider a specific receive beamforming design here only for the purpose of illustrating the effect of BD-IRS reflection.

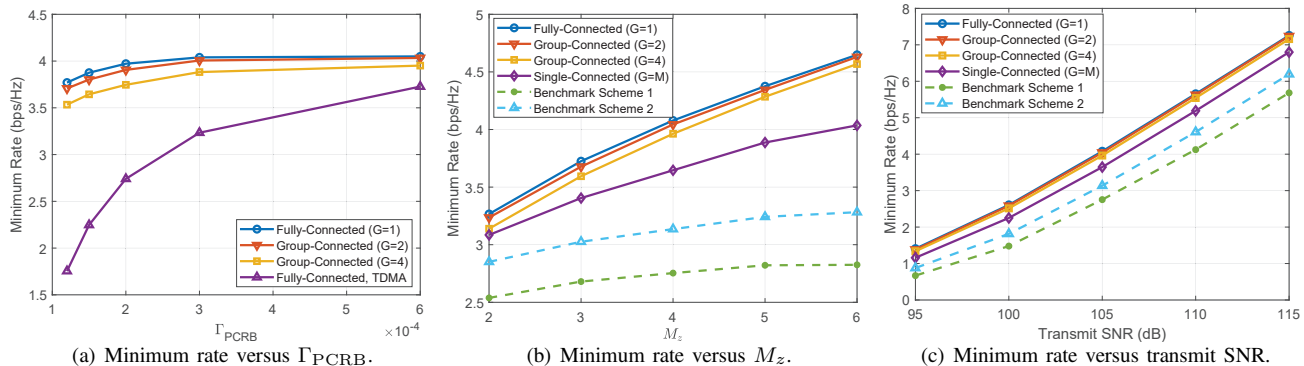


Fig. 6. Minimum rate versus Γ_{PCRB}/M_z /transmit SNR in BD-IRS aided uplink ISAC.

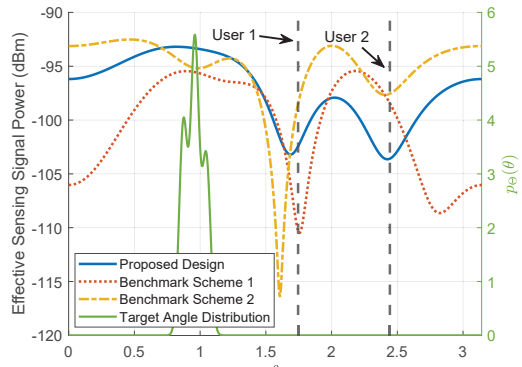


Fig. 7. Effective sensing signal power received at the BS versus θ .

which is the eigenvector corresponding to the largest eigenvalue of $\Sigma_0^{-1} \mathbb{E}_\theta[(\mathbf{R}\Phi\mathbf{g}(\theta))(\mathbf{R}\Phi\mathbf{g}(\theta))^H]$. It can be observed that our proposed design concentrates power towards the angles with high probabilities while suppressing power in the directions of communication users to reduce interference. This validates the effectiveness of our proposed design as well as its gain over the benchmark schemes which cannot achieve the above location-dependent interference management.

D. Comparison of TDMA Versus SDMA

Finally, we consider a scenario with severe interference between sensing and communication, to reveal the potential gain of TDMA over SDMA. Specifically, we set $\theta^{U,1} = \frac{5}{12}\pi$, where the direct user-BS channel is blocked. Note that in this case, user 1 is very close to the highly-probable locations of the target, thereby leading to significant interference. Fig. 8 compares the performance of SDMA via our proposed algorithm for Problem (P1) and TDMA, where both the actual expected rate of SDMA and its approximate lower bound are shown. It is observed that as the sensing requirement becomes less stringent, i.e., Γ_{PCRB} increases, TDMA outperforms SDMA. In this case, more time can be allocated to communication, and the pre-log factor in the TDMA communication rate can be compensated by the larger SINR achieved by removing the interference from sensing. This demonstrates the effectiveness of TDMA in heavy-interference scenarios. In addition, it is observed that the actual expected rate and its lower bound for SDMA are very close, which validates our adoption of the lower bound as the communication performance metric.

VIII. CONCLUSIONS

This paper studied the optimization of BD-IRS reflection in a BD-IRS aided multi-user uplink ISAC system, where the

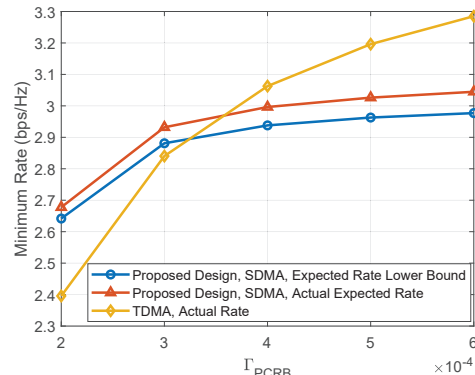


Fig. 8. Comparison between TDMA and SDMA under severe interference.

BS serves multiple uplink users and senses the unknown and random location information of an active target via its sent uplink signals and the location PDF information. The PCRB was firstly derived to characterize the sensing performance and then transformed to a tractable form. Following this, a BD-IRS reflection matrix optimization problem was formulated to maximize the minimum expected rate among multiple users while satisfying a constraint on the PCRB as well as the structural constraints on the reflection matrix. The proposed problem was challenging to solve since it included various types of non-convex components. To address this challenging problem, we proposed a PDD-based algorithm which yields a high-quality suboptimal solution with polynomial-time complexity. We also proposed an alternative TDMA scheme with optimized time allocation. Numerical results validated the effectiveness of the proposed designs and provided useful design insights such as the optimal choice of multiple access scheme. In the future, it is worthwhile extending this work to other emerging new IRS architectures such as active IRS and stacked IRS [8], as well as to cases with joint angle and range estimation and/or multiple sensing targets.

APPENDIX

A. Proof of Proposition 1

Define

$$\bar{\gamma}_k(\mathbf{w}_k, \Phi) \triangleq \frac{P_k |\mathbf{w}_k^H \mathbf{h}_k(\Phi)|^2}{\sum_{\substack{k'=1 \\ k' \neq k}}^K P_{k'} |\mathbf{w}_k^H \mathbf{h}_{k'}(\Phi)|^2 + P_0 \|\mathbf{w}_k^H \mathbf{R} \Phi \mathbf{G}^{\frac{1}{2}}\|^2 + \|\mathbf{w}_k\|^2 \sigma^2} \quad (94)$$

and consequently $\bar{R}_k(\mathbf{w}_k, \Phi) = \log_2(1 + \bar{\gamma}_k(\mathbf{w}_k, \Phi))$ holds. Since $\bar{R}_k(\mathbf{w}_k, \Phi)$ is a monotonically increasing function of

$\bar{\gamma}_k(\mathbf{w}_k, \Phi)$, rate maximization is equivalent to SINR maximization. Since $\bar{\gamma}_k(\mathbf{w}_k, \Phi)$ is independent on $\{\mathbf{w}_{k'}, k' \neq k\}_{k'=1}^K$, the optimization problem of \mathbf{w}_k is given by

$$(\text{P-}w_k) \quad \max_{w_k} \frac{P_k |\mathbf{w}_k^H \mathbf{h}_k(\Phi)|^2}{\mathbf{w}_k^H \Sigma_k(\Phi) \mathbf{w}_k}, \quad (95)$$

where $\Sigma_k(\Phi) = \sum_{k'=1, k' \neq k}^K P_{k'} \mathbf{h}_{k'}(\Phi) \mathbf{h}_{k'}^H(\Phi) + P_0 \mathbf{R} \Phi \mathbf{G} \Phi^H \mathbf{R}^H + \sigma^2 \mathbf{I}_N$. Denote $\mathbf{z}_k = \Sigma_k^{-\frac{1}{2}}(\Phi) \mathbf{w}_k$. Thus, we can express objective of Problem (P- w_k) as

$$\max_{z_k} \frac{P_k \mathbf{z}_k^H \Sigma_k^{-\frac{1}{2}}(\Phi) \mathbf{h}_k(\Phi) \mathbf{h}_k^H(\Phi) \Sigma_k^{-\frac{1}{2}}(\Phi) \mathbf{z}_k}{\mathbf{z}_k^H \mathbf{z}_k}. \quad (96)$$

This problem is a Rayleigh quotient maximization problem and the optimal \mathbf{z}_k^* should align with the eigenvector corresponding to the largest eigenvalue of $\Sigma_k^{-\frac{1}{2}}(\Phi) \mathbf{h}_k(\Phi) \mathbf{h}_k^H(\Phi) \Sigma_k^{-\frac{1}{2}}(\Phi)$ [65]. Therefore, the optimal solution is given by $\mathbf{z}_k^* = \Sigma_k^{-\frac{1}{2}}(\Phi) \mathbf{h}_k(\Phi)$. Then, we have $\mathbf{w}_k = \Sigma_k^{-\frac{1}{2}}(\Phi) \mathbf{z}_k^* = \Sigma_k^{-1}(\Phi) \mathbf{h}_k(\Phi)$. Normalizing \mathbf{w}_k , we obtain the optimal \mathbf{w}_k^* in (10).

B. Proof of Proposition 2

$f_\zeta(\Phi, \nu_\zeta)$ can be rewritten as

$$f_\zeta(\Phi, \nu_\zeta) = \nu_\zeta^H \Sigma_0(\Phi) \nu_\zeta - 2\Re\{\nu_\zeta^H \mathbf{R} \Phi \mathbf{u}_\zeta\} \quad (97)$$

$$= (\nu_\zeta - \Sigma_0^{-1}(\Phi) \mathbf{R} \Phi \mathbf{u}_\zeta)^H \Sigma_0(\Phi) (\nu_\zeta - \Sigma_0^{-1}(\Phi) \mathbf{R} \Phi \mathbf{u}_\zeta) - (\mathbf{R} \Phi \mathbf{u}_\zeta)^H \Sigma_0^{-1}(\Phi) (\mathbf{R} \Phi \mathbf{u}_\zeta). \quad (98)$$

The optimal ν_ζ^* that minimizes $f_\zeta(\Phi, \nu_\zeta)$ is given by

$$\nu_\zeta^* = \Sigma_0^{-1}(\Phi) \mathbf{R} \Phi \mathbf{u}_\zeta. \quad (99)$$

Then, we have

$$f_\zeta(\Phi, \nu_\zeta^*) = -(\mathbf{R} \Phi \mathbf{u}_\zeta)^H \Sigma_0^{-1}(\Phi) (\mathbf{R} \Phi \mathbf{u}_\zeta), \quad (100)$$

$$\sum_{\zeta=1}^R \kappa_\zeta f_\zeta(\Phi, \nu_\zeta^*) = -\sum_{\zeta=1}^R \kappa_\zeta (\mathbf{R} \Phi \mathbf{u}_\zeta)^H \Sigma_0^{-1}(\Phi) (\mathbf{R} \Phi \mathbf{u}_\zeta). \quad (101)$$

Similarly, it can be shown that the optimal ν_k^* to minimize each $f_k(\Phi, \nu_k)$ is given by $\nu_k^* = \Sigma_k^{-1}(\Phi) \mathbf{h}_k(\Phi)$. $f_k(\Phi, \nu_k^*)$ can be further derived as $-\mathbf{h}_k^H(\Phi) \Sigma_k^{-1}(\Phi) \mathbf{h}_k(\Phi)$. The equivalence between Problem (P4-I) and Problem (P4-I-eqv) thus follows by plugging in the values of $f_\zeta(\Phi, \nu_\zeta^*)$ and $f_k(\Phi, \nu_k^*)$ into Problem (P4-I-eqv).

C. Construction of \mathbf{Q}_g

For a given $\Phi_{g,m,n}$, the index of $\Phi_{g,m,n}$ should appear at the $i_2 = (n-1)M_g + m$ -th position of φ_g . Moreover, we define $\widehat{M}_g \triangleq \sum_{g'=1}^{g-1} M_{g'}$ and $\widehat{M}_1 \triangleq 0$. Therefore, the index of $\Phi_{g,m,n}$ in $\text{vec}(\Phi)$ is given by $i_1 = (\widehat{M}_g + n-1)M + \widehat{M}_g + m$. Thus, the $((\widehat{M}_g + n-1)M + \widehat{M}_g + m, (n-1)M_g + m)$ -th entry of \mathbf{Q}_g should be 1. For all (m, n) pairs, we can calculate the corresponding (i_1, i_2) . By denoting the collection of all (i_1, i_2) pairs as \mathcal{I} , the expression of \mathbf{Q}_g is given by $Q_{g,i_1,i_2} = 1$ if $(i_1, i_2) \in \mathcal{I}$ and $Q_{g,i_1,i_2} = 0$ otherwise.

D. Construction of \mathbf{D}_g

The explicit form of \mathbf{D}_g can be expressed as $\mathbf{D}_g = \left(\sum_{m \geq n} e_{mn} (\text{vec}(\mathbf{T}_{mn}))^T \right)^T$ [66], where $e_{mn} \in \mathbb{R}^{\frac{M_g(M_g+1)}{2} \times 1}$, $1 \leq n \leq m \leq M_g$ is a unit vector with element 1 in the $[(n-1)M_g + m - \frac{1}{2}n(n-1)]$ -th position and zeros elsewhere, and $\mathbf{T}_{mn} \in \mathbb{R}^{M_g \times M_g}$ is a matrix with 1 in the (m, n) -th and (n, m) -th position and zeros elsewhere, respectively.

REFERENCES

- [1] S. Zheng and S. Zhang, "BD-IRS aided uplink ISAC exploiting prior information: SDMA or TDMA?" in *Proc. IEEE Int. Wkshps. Signal Process. Adv. Wireless Commun. (SPAWC)*, Jul. 2025.
- [2] L. Liu, S. Zhang, and S. Cui, "Leveraging a variety of anchors in cellular network for ubiquitous sensing," *IEEE Commun. Mag.*, vol. 62, no. 9, pp. 98–104, Sep. 2024.
- [3] F. Liu, Y. Cui, C. Masouros, J. Xu, T. X. Han, Y. C. Eldar, and S. Buzzi, "Integrated sensing and communications: Toward dual-functional wireless networks for 6G and beyond," *IEEE J. Sel. Areas Commun.*, vol. 40, no. 6, pp. 1728–1767, Jun. 2022.
- [4] F. Liu, C. Masouros, A. P. Petropulu, H. Griffiths, and L. Hanzo, "Joint radar and communication design: Applications, state-of-the-art, and the road ahead," *IEEE Trans. Commun.*, vol. 68, no. 6, pp. 3834–3862, Jun. 2020.
- [5] Q. Wu, S. Zhang, B. Zheng, C. You, and R. Zhang, "Intelligent reflecting surface-aided wireless communications: A tutorial," *IEEE Trans. Commun.*, vol. 69, no. 5, pp. 3313–3351, May 2021.
- [6] C. Huang, A. Zappone, G. C. Alexandropoulos, M. Debbah, and C. Yuen, "Reconfigurable intelligent surfaces for energy efficiency in wireless communication," *IEEE Trans. Wireless Commun.*, vol. 18, no. 8, pp. 4157–4170, Aug. 2019.
- [7] M. Di Renzo *et al.*, "Smart radio environments empowered by reconfigurable AI meta-surfaces: An idea whose time has come," *EURASIP J. Wireless Commun. Netw.*, vol. 2019, no. 1, pp. 1–20, Dec. 2019.
- [8] E. Basar *et al.*, "Reconfigurable intelligent surfaces for 6G: Emerging hardware architectures, applications, and open challenges," *IEEE Veh. Technol. Mag.*, vol. 19, no. 3, pp. 27–47, Sep. 2024.
- [9] S. Zhang and R. Zhang, "Capacity characterization for intelligent reflecting surface aided MIMO communication," *IEEE J. Sel. Areas Commun.*, vol. 38, no. 8, pp. 1823–1838, Aug. 2020.
- [10] Y. Yang, B. Zheng, S. Zhang, and R. Zhang, "Intelligent reflecting surface meets OFDM: Protocol design and rate maximization," *IEEE Trans. Commun.*, vol. 68, no. 7, pp. 4522–4535, Jul. 2020.
- [11] S. Zheng, B. Lv, T. Zhang, Y. Xu, G. Chen, R. Wang, and P. C. Ching, "On DoF of active RIS-assisted MIMO interference channel with arbitrary antenna configurations: When will RIS help?" *IEEE Trans. Veh. Technol.*, vol. 72, no. 12, pp. 16 828–16 833, Dec. 2023.
- [12] R. Liu, M. Li, H. Luo, Q. Liu, and A. L. Swindlehurst, "Integrated sensing and communication with reconfigurable intelligent surfaces: Opportunities, applications, and future directions," *IEEE Wireless Commun.*, vol. 30, no. 1, pp. 50–57, Feb. 2023.
- [13] S. P. Chepuri, N. Shlezinger, F. Liu, G. C. Alexandropoulos, S. Buzzi, and Y. C. Eldar, "Integrated sensing and communications with reconfigurable intelligent surfaces: From signal modeling to processing," *IEEE Signal Process. Mag.*, vol. 40, no. 6, pp. 41–62, Sep. 2023.
- [14] X. Wang, Z. Fei, J. Huang, and H. Yu, "Joint waveform and discrete phase shift design for RIS-assisted integrated sensing and communication system under Cramer-Rao bound constraint," *IEEE Trans. Veh. Technol.*, vol. 71, no. 1, pp. 1004–1009, Jan. 2022.
- [15] Q. Wang, L. Liu, S. Zhang, B. Di, and F. C. M. Lau, "A heterogeneous 6G networked sensing architecture with active and passive anchors," *IEEE Trans. Wireless Commun.*, vol. 23, no. 8, pp. 9502–9517, Aug. 2024.
- [16] M. Hua, Q. Wu, W. Chen, O. A. Dobre, and A. L. Swindlehurst, "Secure intelligent reflecting surface-aided integrated sensing and communication," *IEEE Trans. Wireless Commun.*, vol. 23, no. 1, pp. 575–591, Jan. 2024.
- [17] Y. Liu and W. Yu, "RIS-assisted joint sensing and communications via fractionally constrained fractional programming," in *Proc. IEEE Global Commun. Conf. (GLOBECOM)*, Dec. 2024, pp. 650–655.

- [18] Z. Wang, X. Mu, and Y. Liu, "STARS enabled integrated sensing and communications," *IEEE Trans. Wireless Commun.*, vol. 22, no. 10, pp. 6750–6765, Oct. 2023.
- [19] H. Li, S. Shen, M. Nerini, and B. Clerckx, "Reconfigurable intelligent surfaces 2.0: Beyond diagonal phase shift matrices," *IEEE Commun. Mag.*, vol. 62, no. 3, pp. 102–108, Mar. 2024.
- [20] S. Shen, B. Clerckx, and R. Murch, "Modeling and architecture design of reconfigurable intelligent surfaces using scattering parameter network analysis," *IEEE Trans. Wireless Commun.*, vol. 21, no. 2, pp. 1229–1243, Feb. 2022.
- [21] D. Wijekoon, A. Mezghani, G. C. Alexandropoulos, and E. Hossain, "Physically-consistent modeling and optimization of non-local RIS-assisted multi-user MIMO communication systems," 2024. [Online]. Available: <https://arxiv.org/abs/2406.05617>.
- [22] A. Mezghani, F. Bellili, and E. Hossain, "Reconfigurable intelligent surfaces for quasi-passive mmWave and THz networks: Should they be reflective or redirective?" in *Proc. IEEE Conf. Asilomar Conf. Signals, Syst., Comput.*, Oct. 2022, pp. 1076–1080.
- [23] M. Nerini, S. Shen, H. Li, and B. Clerckx, "Beyond diagonal reconfigurable intelligent surfaces utilizing graph theory: Modeling, architecture design, and optimization," *IEEE Trans. Wireless Commun.*, vol. 23, no. 8, pp. 9972–9985, Aug. 2024.
- [24] H. Li, S. Shen, and B. Clerckx, "Beyond diagonal reconfigurable intelligent surfaces: From transmitting and reflecting modes to single-, group-, and fully-connected architectures," *IEEE Trans. Wireless Commun.*, vol. 22, no. 4, pp. 2311–2324, Apr. 2023.
- [25] —, "Beyond diagonal reconfigurable intelligent surfaces: A multi-sector mode enabling highly directional full-space wireless coverage," *IEEE J. Sel. Areas Commun.*, vol. 41, no. 8, pp. 2446–2460, Aug. 2023.
- [26] H. Li, S. Shen, M. Nerini, M. Di Renzo, and B. Clerckx, "Beyond diagonal reconfigurable intelligent surfaces with mutual coupling: Modeling and optimization," *IEEE Commun. Lett.*, vol. 28, no. 4, pp. 937–941, Apr. 2024.
- [27] Y. Zhou, Y. Liu, H. Li, Q. Wu, S. Shen, and B. Clerckx, "Optimizing power consumption, energy efficiency, and sum-rate using beyond diagonal RIS—a unified approach," *IEEE Trans. Wireless Commun.*, vol. 23, no. 7, pp. 7423–7438, Jul. 2024.
- [28] K. D. Katsanos, P. D. Lorenzo, and G. C. Alexandropoulos, "Multi-RIS-empowered multiple access: A distributed sum-rate maximization approach," *IEEE J. Sel. Topics Signal Process.*, vol. 18, no. 7, pp. 1324–1338, Oct. 2024.
- [29] H. Li, S. Shen, and B. Clerckx, "Synergizing beyond diagonal reconfigurable intelligent surface and rate-splitting multiple access," *IEEE Trans. Wireless Commun.*, vol. 23, no. 8, pp. 8717–8729, Aug. 2024.
- [30] M. Soleymani, I. Santamaria, E. A. Jorswieck, and B. Clerckx, "Optimization of rate-splitting multiple access in beyond diagonal RIS-assisted URLLC systems," *IEEE Trans. Wireless Commun.*, vol. 23, no. 5, pp. 5063–5078, May 2024.
- [31] A. M. Huroon, Y.-C. Huang, and L.-C. Wang, "Optimized transmission strategy for UAV-RIS 2.0 assisted communications using rate splitting multiple access," in *Proc. IEEE 98th Veh. Technol. Conf. (VTC) Fall*, Oct. 2023, pp. 1–6.
- [32] A. Mahmood, T. X. Vu, W. U. Khan, S. Chatzinotas, and B. Ottersten, "Joint computation and communication resource optimization for beyond diagonal UAV-RIS empowered MEC networks," 2024. [Online]. Available: <https://arxiv.org/abs/2311.07199>.
- [33] T. D. Hua, M. Mohammadi, H. Q. Ngo, and M. Matthaiou, "Cell-free massive MIMO SWIPT with beyond diagonal reconfigurable intelligent surfaces," in *Proc. IEEE Wireless Commun. Netw. Conf. (WCNC)*, Apr. 2024, pp. 1–6.
- [34] S. Lin, Y. Zou, Y. Jiang, L. Yang, Z. Cui, and L.-N. Tran, "Securing FC-RIS and UAV empowered multiuser communications against a randomly flying eavesdropper," *IEEE Wireless Commun. Lett.*, vol. 14, no. 2, pp. 255–259, Feb. 2025.
- [35] Q. Zhang, G. Luo, Z. Dong, F. Sun, X. Wang, and J. Liu, "Beyond-diagonal reconfigurable intelligent surface enhanced NOMA systems," *IEEE Wireless Commun. Lett.*, vol. 14, no. 1, pp. 118–122, Jan. 2025.
- [36] Z. Liu, Y. Liu, S. Shen, Q. Wu, and Q. Shi, "Enhancing ISAC network throughput using beyond diagonal RIS," *IEEE Wireless Commun. Lett.*, vol. 13, no. 6, pp. 1670–1674, Jun. 2024.
- [37] Z. Guang, Y. Liu, Q. Wu, W. Wang, and Q. Shi, "Power minimization for ISAC system using beyond diagonal reconfigurable intelligent surface," *IEEE Trans. Veh. Technol.*, vol. 73, no. 9, pp. 13 950–13 955, Sep. 2024.
- [38] T. Esmailbeig, K. V. Mishra, and M. Soltanalian, "Beyond diagonal RIS: Key to next-generation integrated sensing and communications?" *IEEE Signal Process. Lett.*, vol. 32, pp. 216–220, Dec. 2025.
- [39] B. Wang, H. Li, S. Shen, Z. Cheng, and B. Clerckx, "A dual-function radar-communication system empowered by beyond diagonal reconfigurable intelligent surface," *IEEE Trans. Commun.*, vol. 73, no. 3, pp. 1501–1516, Mar. 2025.
- [40] Y. Zhang, X. Shao, H. Li, B. Clerckx, and R. Zhang, "Full-space wireless sensing enabled by multi-sector intelligent surfaces," *IEEE Trans. Wireless Commun.*, 2025, Early Access.
- [41] K. Chen and Y. Mao, "Transmitter side beyond-diagonal RIS for mmWave integrated sensing and communications," in *Proc. IEEE Int. Wkshps. Signal Process. Adv. Wireless Commun. (SPAWC)*, Sep. 2024, pp. 951–955.
- [42] C. Xu and S. Zhang, "MIMO integrated sensing and communication exploiting prior information," *IEEE J. Sel. Areas Commun.*, vol. 42, no. 9, pp. 2306–2321, Sep. 2024.
- [43] K. Hou and S. Zhang, "Optimal beamforming for secure integrated sensing and communication exploiting target location distribution," *IEEE J. Sel. Areas Commun.*, vol. 42, no. 11, pp. 3125–3139, Nov. 2024.
- [44] X. Du, S. Zhang, and L. Liu, "UAV trajectory optimization for sensing exploiting target location distribution map," in *Proc. IEEE 99th Veh. Technol. Conf. (VTC) Spring*, Jun. 2024, pp. 1–5.
- [45] C. Xu and S. Zhang, "Integrated sensing and communication exploiting prior information: How many sensing beams are needed?" in *Proc. IEEE Int. Symp. Inf. Theory (ISIT)*, Jul. 2024, pp. 2802–2807.
- [46] J. Yao and S. Zhang, "Optimal beamforming for multi-target multi-user ISAC exploiting prior information: How many sensing beams are needed?" 2025. [Online]. Available: <https://arxiv.org/abs/2503.03560>.
- [47] Y. Wang and S. Zhang, "Hybrid beamforming design for integrated sensing and communication exploiting prior information," in *Proc. IEEE Global Commun. Conf. (Globecom)*, Dec. 2024, pp. 4576–4581.
- [48] C. Xu and S. Zhang, "MIMO radar transmit signal optimization for target localization exploiting prior information," in *Proc. IEEE Int. Symp. Inf. Theory (ISIT)*, Jun. 2023, pp. 310–315.
- [49] J. Yao and S. Zhang, "Optimal transmit signal design for multi-target MIMO sensing exploiting prior information," in *Proc. IEEE Global Commun. Conf. (Globecom)*, Dec. 2024, pp. 4920–4925.
- [50] K. Hou and S. Zhang, "Secure integrated sensing and communication exploiting target location distribution," in *Proc. IEEE Global Commun. Conf. (Globecom)*, Dec. 2023, pp. 4933–4938.
- [51] K. M. Attiah and W. Yu, "Beamforming design for integrated sensing and communications using uplink-downlink duality," in *Proc. IEEE Int. Symp. Inf. Theory (ISIT)*, Jul. 2024, pp. 2808–2813.
- [52] W. Zhu, S. Zhang, and L. Liu, "Joint transmission and compression optimization for networked sensing with limited-capacity fronthaul links," *IEEE Trans. Wireless Commun.*, 2025, Early Access.
- [53] Q. Shi and M. Hong, "Penalty dual decomposition method for non-smooth nonconvex optimization—Part I: Algorithms and convergence analysis," *IEEE Trans. Signal Process.*, vol. 68, pp. 4108–4122, Jun. 2020.
- [54] Q. Shi, L. Liu, S. Zhang, and S. Cui, "Device-free sensing in OFDM cellular network," *IEEE J. Sel. Areas Commun.*, vol. 40, no. 6, pp. 1838–1853, Jun. 2022.
- [55] L. Yan, Y. Chen, C. Han, and J. Yuan, "Joint inter-path and intra-path multiplexing for terahertz widely-spaced multi-subarray hybrid beamforming systems," *IEEE Trans. Commun.*, vol. 70, no. 2, pp. 1391–1406, Feb. 2022.
- [56] H. Li, S. Shen, and B. Clerckx, "A dynamic grouping strategy for beyond diagonal reconfigurable intelligent surfaces with hybrid transmitting and reflecting mode," *IEEE Trans. Veh. Technol.*, vol. 72, no. 12, pp. 16748–16753, Dec. 2023.
- [57] H. Li, S. Shen, Y. Zhang, and B. Clerckx, "Channel estimation and beamforming for beyond diagonal reconfigurable intelligent surfaces," *IEEE Trans. Signal Process.*, vol. 72, pp. 3318–3332, Jul. 2024.
- [58] R. Wang, S. Zhang, B. Clerckx, and L. Liu, "Low-overhead channel estimation framework for beyond diagonal reconfigurable intelligent surface assisted multi-user MIMO communication," 2025. [Online]. Available: <https://arxiv.org/abs/2504.10911>.
- [59] R. Wang, S. Zhang, and L. Liu, "Low-overhead channel estimation for beyond diagonal reconfigurable intelligent surface aided single-user communication," in *Proc. IEEE Int. Conf. Wireless Commun. Signal Process. (WCSP)*, Oct. 2024, pp. 305–310.
- [60] H. L. Van Trees, *Detection, Estimation, and Modulation Theory: Part I*. New York, USA: Wiley, 1968.
- [61] G. A. Seber, *A Matrix Handbook for Statisticians*. Hoboken, NJ, USA: Wiley, 2008.
- [62] A. Ben-Tal and A. Nemirovski, *Lectures on Modern Convex Optimization: Analysis, Algorithms, and Engineering Applications*. Philadelphia, PA, USA: SIAM, 2001.

- [63] M. Grant and S. Boyd. (Jun. 2015). *CVX: MATLAB Software for Disciplined Convex Programming*. [Online]. Available: <http://cvxr.com/cvx/>
- [64] J. Manton, "Optimization algorithms exploiting unitary constraints," *IEEE Trans. Signal Process.*, vol. 50, no. 3, pp. 635–650, Mar. 2002.
- [65] R. A. Horn and C. R. Johnson, *Matrix Analysis*. Cambridge, U.K.: Cambridge Univ. Press, 2013.
- [66] J. R. Magnus and H. Neudecker, "The elimination matrix: Some lemmas and applications," *SIAM J. Algebr. Discrete Methods*, vol. 1, no. 4, pp. 422–449, 1980.